Supernovae interacting with their Circumstellar Medium

Master Thesis of Bob van Veelen

Supervised by Dr. N. Langer

Abstract

During the lifetime of a massive star, its wind has important effects on the evolution of its Circumstellar Medium (CSM). The stellar wind creates a large bubble of low density and one or more shells with higher density. At the end of the stellar life, the star explodes and the evolution of the supernova remnant will be affected by this CSM evolution. The interaction of the supernova ejecta with the CSM may give rise to features which might not occur when assuming a uniform ambient medium. It is therefor important to not only model the interaction of the SN ejecta with the CSM itself but also the pre-supernova CSM evolution. In this thesis a method for simulating the pre-supernova evolution of the CSM and the interaction of the supernova ejecta with the CSM is developed. This method is applied to two cases. The first case concerns the late time observation of SN 2001em, which showed a rebrightening in the X-ray and radio flux. With the second case we investigate a single star progenitor model for the Cas A SNR. The conclusions for the first case were that our method was giving us results which were similar to results obtained using a different method. The obtained results also reproduced the observations of the late time high X-ray luminosity. The conslusions for the second case were that the adopted single star model is a viable option for the progenitor of Cas A. The results also showed a strong correspondance of an observational feature in Cas A, which could be linked to parts of our results.

Contents

List of Figures

Chapter 1

Introduction

Supernovae are among the most violent events in the universe. For a brief moment a supernova can be as bright as the galaxy it resides in. Due to the technological advances, the number of detected supernovae has increased enormously. As a result of this our knowledge of supernovae has also increased.

Continuously during the evolution of a massive star, it burns material in its center to replenish the energy which is lost at the surface of the star, due to the emission of light and neutrinos. In the burning process atomic nuclei are fused into new nuclei. The total mass of these new nuclei is smaller than the total mass of the old ones, and the difference in mass is converted into energy.

There are a number of burning phases in the stellar life. During the largest part of the life of the star it is burning hydrogen into helium in its core. This phase is called the Main Sequence (MS) phase. After this the star will again burn hydrogen into helium but now not in the core of the star but in a shell around the core. This phase is called the Red Super Giant (RSG) phase. During this phase the core contracts and helium in the core will be burnt into carbon and oxygen. After the core helium burning phase, it has only a very short amount of time to live compared to the time it spends in the core hydrogen burning phase. If the star is a massive one at the start of its evolution, bigger than approximately 9 solar masses ($M_{\odot}$), the burning phases will continue in the star until the most central part of the core has been burnt to iron. With each consecutive burning phase of the core, a smaller part will take part in the burning process. The result is an iron core, and when moving outward from the center there will be mantles with lighter elements. This model is called the onion skin model and can be seen in Figure 1.1. For a more thorough and exact explanation about stellar evolution we refer to Kippenhahn & Weigert (1990)

At the end of the evolution of the star the iron core cannot be burnt further to gain more energy. Since the star is still emitting light it needs

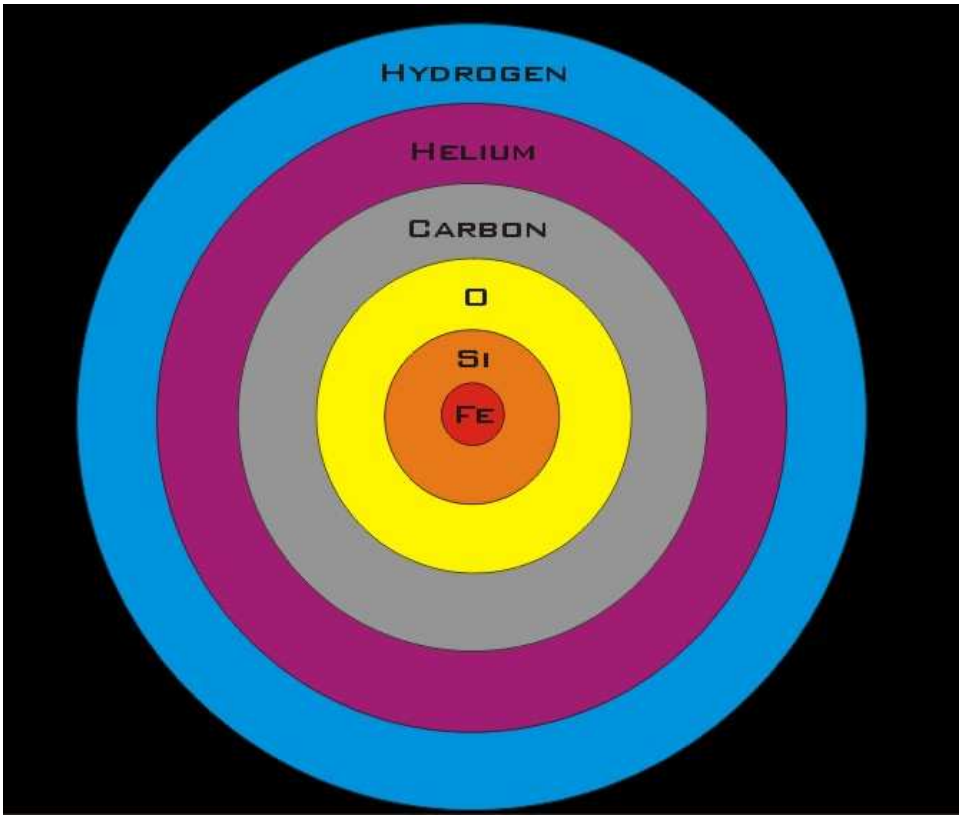

Figure 1.1: The onion skin model for a star at the end of its life. Moving from the inside of the star outward, one finds mantles with atomic nuclei decreasing in mass. The scaling of the figure is not real. Image credits: Carolyn Brinkworth and Claire Thomas.

to gain energy. The stellar core can now only gain energy by contracting. As a consequence the temperature and pressure in the core will increase. The material in the center of the star will start to disintegrate into lighter elements. This process costs energy and this will force the star to shrink its core even more towards higher pressures and temperatures. The result is a catastrophic runaway process in which the core collapses, which will finally result in the explosion of the star (Kippenhahn & Weigert 1990). If a star explodes in this manner the supernova is called a core collapse supernova. What happens between the time at which the core collapses and the time at which the mass and energy are ejected in the supernova explosion is not completely understood yet. Nevertheless it is clear that mass and energy *are* ejected.

Core collapse supernovae are divided into several different classes, Type Ib, Type Ic and Type II (da Silva 1993). The classification of these different

sorts of supernovae is done with help of their spectra and light curves. If the spectrum of a supernova shows hydrogen the supernova is of Type II. If the supernova spectrum does not show any hydrogen or silicon then it is of Type Ib or Ic. When considering a Type Ib supernova, the presence of helium can be seen from the spectrum, and in the case of a Type Ic there is no helium visible.

Next to the core collapse supernovae there are also supernovae Type Ia. These supernovae originate from binaries, systems in which two stars orbit around each other (Nomoto et al. 1984). When two stars are in an orbit around each other and the stellar evolution causes one of the stars to expand, it is possible that part of the mass of one star is transferred to the other star. If the star that is receiving mass is a white dwarf, a star which originally was not very massive and now is at the end of its life, it may reach a point at which the white dwarf cannot sustain the inward pointing force from gravity. When this happens the star also ends up as a supernova. In this case the spectrum of the supernova shows no hydrogen but does show the presence of silicon. The mechanism with which these stars become supernovae is, just as with the core collapse supernovae, not yet fully understood but is distinctly different from the core collapse supernovae. While in core collapse supernovae the energy for the explosion is provided by the collapsing core, in Type Ia supernovae, the energy comes from explosive burning. This is also the reason that they are called thermonuclear supernovae.

A stellar core collapse obviously has dramatic effects on the star itself, but next to this it also has a large effect on the surrounding medium. The surroundings of a star is already changed during the stellar evolution, due to effects of a stellar wind and radiation. If the star is a massive one, its wind can create a large cavity in the Circumstellar Medium (CSM), sweeping up a dense shell around it. Weaver et al. (1977) show that, when certain assumptions are made, there are analytic solutions for the structure of the CSM. The wind parameters for the star have to be constant, the density of the surrounding medium has to be constant and the kinetic energy injected into the surroundings by the star, cannot be lost. In this simplified picture the structure of the CSM can be separated into four distinct regions (Figure 1.2). The solutions from this paper describe the values for pressure, density and radius of region b and c as a function of the wind parameters, time and density of the surrounding medium. The region with the shocked stellar wind is also called the hot bubble, since the density in this region is very low and the temperature very high. The transition at R_c is called a contact discontinuity. This is a transition along which the pressure on both sides is equal but the density changes.

In reality the star evolves during its life and as a result the wind parameters change. The biggest changes occur when a star evolves from one phase to another during its evolution. For instance when the star goes from the MS phase to the RSG phase. To get a more realistic view of the structure of

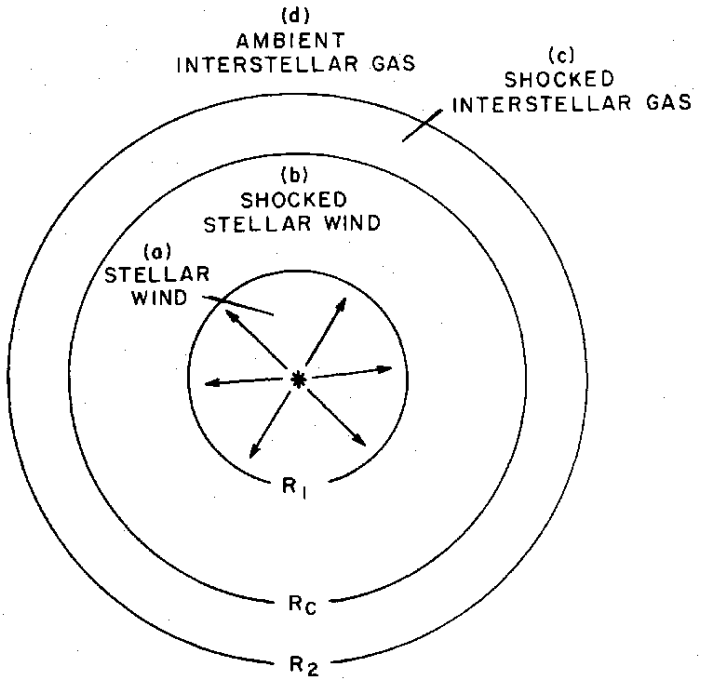

Figure 1.2: Structure of the CSM for a star with constant wind parameters during its entire stellar life. The ambient medium, at the start of the stellar life, also has to be uniform. Located at R_1 and R_2 are shocks separating the shocked matter from the unshocked mater. At R_c there is a density jump, separating the shocked stellar wind from the shocked ambient medium. Figure taken from Weaver et al. (1977).

the CSM, one has to take this into consideration. When considering more than one dimension there are effects on the evolution of the CSM. In two dimensions, hydrodynamical instabilities can occur, which can not occur in one dimensional calculations.

Instabilities like thin shell instabilities (Ryu & Vishniac 1988) and Rayleigh Taylor instabilities (Allen & Hughes 1984) can only occur when calculating in two or three dimensions. These are the instabilities which occur the most frequent when considering stellar winds and supernova explosions. Thin shell instabilities occur when a shell is held together by pressure from both sides and the pressure on one side of the shell is not isotropic. Rayleigh-Taylor instabilities occur when a dense gas is accelerated by a less dense gas. Multi dimensional studies of CSM evolution, including the detailed effects of stellar evolution on the wind parameters, have been done by Garcia-Segura et al. (1996 a,b). Here time dependent wind parameters are taken into account, and because the calculations are done in more than one dimension the effect of instabilities can be seen.

The explosion of a star within a simplified (constant density) surrounding medium has been described by Woltjer (1972) and Chevalier (1977). The evolution of the supernova remnant can then be described by several stages. These stages are distinguished by the velocity with which the supernova remnant expands into the surrounding medium. This speed is constantly decreasing because the ejected mass of the supernova sweeps up more and more of its surroundings. The mass that is swept up, will be swept up in a shell.

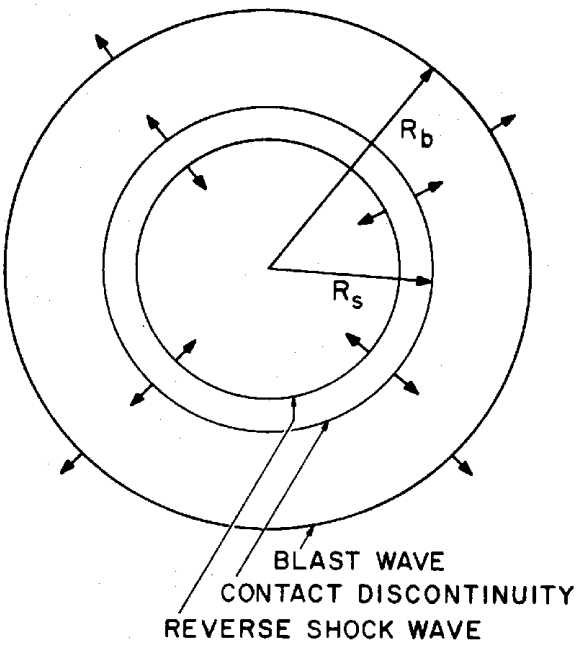

Figure 1.3: Structure of a SNR in the ST phase. The blast wave, located at R_b and moving outward, the reverse shock moving inward and the contact discontinuity, located at R_s and separates the shocked supernova ejecta from the shocked ambient medium, are shown.

The first two stages are the ejecta dominated (ED) phase and the Sedov-Taylor (ST) phase. In the ejecta dominated phase, the expansion of the supernova remnant is hardly influenced by the surrounding medium. In this case the momentum of the supernova ejecta is driving the expansion of the SNR. When the amount of ambient medium mass swept up in the shell by the expanding supernova remnant becomes comparable to the amount of supernova ejecta mass in the shell, the supernova remnant enters the Sedov-Taylor phase. A large part of the energy from the supernova explosion will be put into the surrounding medium and some of this energy will be lost through the emission of light. These processes slow down the expansion of the remnant. In the ST phase the expansion of the SNR is driven by a

combination of the momentum of the unshocked supernova ejecta and the pressure from the shocked supernova ejecta. The structure of the supernova remnant in the ST phase can be separated into several regions, which are shown in Figure 1.3.

The figure shows the blast wave, or forward shock, moving outward and preceding the supernova ejecta. This blast wave accelerates the ambient medium and increases the temperature of the shocked material. The matter between R_s and R_b consists of shocked ambient medium. Everything within R_s is supernova ejecta, but only the part between R_s and the reverse shock is shocked supernova ejecta. The contact discontinuity separates the shocked ejecta from the shocked ambient medium. The reverse shock is moving inward with respect to the supernova ejecta, and decelerates and heats the matter it shocks. At the end of the ST phase all the ejecta has been shocked and the supernova remnant enters the pressure driven snowplow phase. In this phase only the gas pressure from the shocked supernova ejecta is driving the expansion of the SNR.

A nice example of a supernova where the structure of the surrounding has been important in its evolution is SN1987A (Meyer 1997). During the stellar evolution of the progenitor star, the stellar wind created a high density shell relatively close to the star. Some years after the initial explosion the ejecta from the supernova explosion started to collide with this shell and this collision increased its temperature. The heating of this shell caused it to start emitting a large amount of light which we can see. A compilation of images over a time span of 10 years seen in Figure 1.4 show the shell rebrightening.

The goal of the presented research was to put constraints on the evolution of the progenitor stars and the evolution of their CSM, of observed supernova remnants, by using a numerical hydrodynamical code. To do this we implement a way to reproduce a supernova explosion, i.e the supernova ejecta, and combine this with results of the evolution of the CSM of the progenitor star.

This method is shown in Chapter 2. After this we compared the results of our model with the results of another model for the progenitor evolution of SN 2001em, and in the mean time, compare the results of our model with the observations of this supernova. The results of this are shown in Chapter 3. Finally we want to be able to use this method to reach the goal mentioned above. We chose a progenitor model for the Cas A supernova remnant, and simulated this with help of the developed method. The results of this are shown in Chapter 4. And finally in Chapter 5 we discuss the results and conclude.

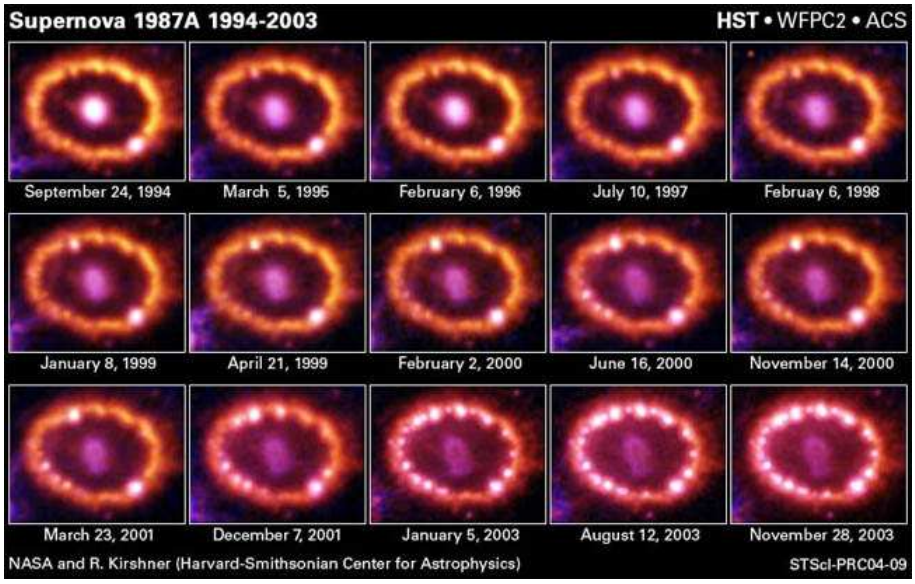

Figure 1.4: SN1987A through the years. The collision of the supernova ejecta with a high density shell, which was formed by the stellar wind of the progenitor star, causes the shell to rebrighten. The shell can be seen as an elliptical ring. In a time span of approximately 10 years the shell is starting to emit more and more light due to this collision. These pictures were taken in the optical wavelength regime. Image credit: NASA/STScI

Chapter 2

Method

2.1 The Code

All the simulations of this thesis are performed with the ZEUS3D code, which is based on ZEUS2D described in Stone & Norman (1992). This is a three dimensional Newtonian magneto-hydrodynamics code, which solves the Euler equations on a staggered mesh grid with help of the following formulas:

$$\frac{\partial \rho}{\partial t} = -\nabla \cdot (\rho \mathbf{v}) \ , \tag{2.1}$$

$$\frac{\partial \mathbf{S}}{\partial t} = -\nabla(\mathbf{S}\mathbf{v}) - \nabla \mathrm{P} \ , \tag{2.2}$$

$$\frac{\partial e}{\partial t} = -\nabla \cdot (e\mathbf{v}) - \mathrm{P}\nabla \cdot \mathbf{v} \ , \tag{2.3}$$

where ρ is the gas density, $\mathbf{v}$ is the velocity vector, $\mathbf{S}$ is the momentum vector, P is the thermal gas pressure and e is the internal energy density per unit volume. It is assumed in the code that all the gas can be described with the ideal gas equation of state.

Equation 2.1 is the mass continuity equation and describes the in- and outflow of gas in a volume. The next equation is the momentum conservation equation. The change in the momentum in a volume depends on change of the momentum of the matter inside and on the thermal pressure gradient of the gas. The last equation shows the change of the internal energy by mass entering and leaving the volume and the compression or expansion of the gas. Magnetism and gravity are also in the ZEUS3D code but are not used here. Radiative energy loss can be included in the code, and this changes the left side of Equation 2.3 to:

$$\left(\frac{\partial e}{\partial t}\right) - n_e n_H \Lambda(T) \ . \tag{2.4}$$

Here $\Lambda(T)$ is a cooling function taken from MacDonald & Bailey (1981), and n_e and n_H are the number densities for electrons and hydrogen particles. The hydrogen particle number density consists of both the ionized and the not ionized hydrogen particles. To be able to calculate number densities, we assumed that all the gas consists of hydrogen.

A cooling function defines the amount of energy lost through radiation as a function of temperature, composition and ionization fraction. The code does not track elemental abundances, which means we are only able to use the temperature for determining the value of the cooling function. The cooling curve used in MacDonald & Bailey (1981) is combined from a number of other papers, extrapolated below 10^4 K and above 10^8 K. Only cooling by bremsstrahlung is considered above 10^8 K. The cooling curve is equal to 0 at 100 K, which means that below 100 K only adiabatic cooling will be able to cool the gas.

Photo-ionization can also be included in the simulations. This option was not available in the code originally. We used the same routine as in García-Segura et al. (1999). The photo-ionization is determined by calculating the Stömgren radius for each radial grid line. The number of photons needed to ionize each grid cell along that radial grid line is determined and with a fixed number of ionizing photons this gives the Strömgren radius. It is assumed that everything within the Strömgren radius is ionized and everything outside the Strömgren radius is not ionized. When a grid cell is ionized it is assumed it is *fully* ionized which means n_e and n_H are equal, and n_H is just the number of protons. Throughout this thesis the photo-ionization will be referred to as ionization.

In theory the cooling curve would not apply if the grid cell was not ionized, since there are no electrons at that point, but nevertheless the cooling curve is also applied for the not ionized grid cells. Since hydrogen is almost completely ionized at 10^4 K and and the cooling function peaks above 10^4 K, the inclusion of cooling for not ionized gas will not have a large influence. It is possible to modify the cooling curve such that the amount of radiative cooling is equal to 0 below 10^4 K. Only adiabatic cooling would occur below 10^4 K if this would be done. For simplicity we did not modify the cooling curve.

To be able to treat shocks, in the ZEUS3D code, artificial viscosity is used. This means that shocks will not occupy a single grid cells, but will be smeared out over a number of grid cells. This is done because ZEUS3D cannot handle infinitesimally thin shocks. The shocks which occur in our results will thus be smeared out over a number of grid cells.

2.2 Computing the CSM of Supernovae

The hydrodynamical interaction of stellar winds, which change during the stellar life, with the Circumstellar Medium (CSM) have to be done numerically. Especially when the star goes through several different phases, for instance from the MS to the RSG phase, the hydrodynamical interaction of the winds with the CSM has to be done numerically. The important parameters for stellar winds are the mass loss rate and the terminal velocity of the wind. To simulate the wind interacting with the CSM we used the method which is also described in Garcia-Segura et al. (1996). In this method the five innermost grid cells are filled with a density and velocity according to $\rho = \frac{\dot{M}}{4\pi r^2 v}$. in which $\dot{M}$ is the mass loss rate, v is the terminal wind velocity and r is the distance from the center. These values are set in every time step done by ZEUS3D, which makes the inflowing stellar wind time dependent.

Because computing the hydrodynamical interactions of stellar winds with the CSM is very time consuming we made approximations. The interaction of the MS and RSG winds with the CSM were not calculated. In stead we assumed that the part of the CSM we were considering only consisted of the free streaming RSG wind, for which we could derive the density and velocity with help of the mass loss rate and terminal wind velocity. These assumptions saved considerable computing time.

2.3 Description of the Supernova Ejecta

We assume that the following density, and velocity law are valid for the supernova ejecta.

$$\rho(v,t) = \begin{cases} F \cdot t^{-3} & \text{for} \quad v \leq v_{core} \\ F \cdot t^{-3} \cdot (\frac{v}{v_{core}})^{-n} & \text{for} \quad v > v_{core} \end{cases} , \tag{2.5}$$

$$v(r,t) = \frac{r}{t} \quad \text{for} \quad t > 0 \ , \tag{2.6}$$

where ρ is the density, t is the time, v is the velocity and r is the radius. F and v_{core} are normalization constants which have to be determined. The density is dependent on both the time and velocity. The expansion of the ejecta causes the volume to increase with r^3, so the density decreases with $r^{-3} \sim t^{-3}$. At a specific time the density is only dependent on the velocity. The dependence of the density on the velocity can be described in two parts. The inner part of the supernova ejecta ($v \leq v_{core}$) has a constant density and the density in the outer part ($v > v_{core}$) decreases exponentially with an index n. Such a density profile is usually assumed for core collapse supernovae (Dwarkadas 2005; Chugai & Chevalier 2006; Truelove & McKee 1999).

The value of the index n is dependent on the density structure of the progenitor star. Matzner & McKee (1999) find that a RSG progenitor will give a index of $n = 11.7$, while if the progenitor star is more compact, because it has a radiative mantle, the index will decrease to $n = 10.2$. In a progenitor star which is more compact the density at the surface will be higher. The matter at the surface will get the maximum velocity, and thus the profile will be shallower, which results in a lower index. For simplicity we chose not to vary the value of n, but chose a constant value of 9.

An explanation for the assumed profile can be found in Matzner & McKee (1999). There it is shown that at some time after the initial blast, the ejecta density profile can be approximated to a profile with flat inner core and a steeply declining outer edge, which is the assumed density profile. The assumed density profile is not valid during the explosion. During the supernova explosion a lot of violent and dynamic interactions take place within the star, which cannot be approximated with the assumed density profile.

Two parameters have to be determined when using the assumed density profile: v_{core} and F. The total mass and energy have to agree with the supernova parameters, the ejecta mass (M_{ej}) and energy (E_{ej}), which one can choose. All the energy is assumed to be kinetic energy. The parameters can be computed in the following manner. Choose a radius ($r_0 > 0$) and a time at which the last part of the ejecta has passed this chosen radius (t_{max}). At r_0 the mass- and energy flux have to be determined and integrated over time. This gives the following equations:

$$E_{ej} = \int_0^{t_{max}} 4\pi r_0^2 \cdot \frac{1}{2}\rho(v,t)v(t)^2 \cdot v(t)\mathrm{d}t \ , \tag{2.7}$$

$$M_{ej} = \int_0^{t_{max}} 4\pi r_0^2 \cdot \rho(v,t) \cdot v(t)\mathrm{d}t \ . \tag{2.8}$$

If one now inserts Equation (2.5) and (2.6) into Equation (2.7) and (2.8) the following equations are obtained:

$$M_{ej} = 4\pi r_0^3 F \left(\left(\frac{t_{core}^{-n}}{n-3} \right) (t_{core}^{n-3} - t_{min}^{n-3}) - \frac{1}{3}(t_{max}^{-3} - t_{core}^{-3}) \right) \ , \tag{2.9}$$

$$E_{ej} = 2\pi r_0^5 F \left(\left(\frac{t_{core}^{-n}}{n-5} \right) (t_{core}^{n-5} - t_{min}^{n-5}) - \frac{1}{5}(t_{max}^{-5} - t_{core}^{-5}) \right) \ . \tag{2.10}$$

Here t_{min} and t_{max} correspond to the times at which the first and last part of ejecta pass r_0, and $t_{core} = r_0/v_{core}$. If $n > 5$, $t_{min} << t_{core}$ and $t_{max} >>$

t_{core} one can approximate Equations 2.9 and 2.10, by setting $t_{min}^{n-5} = 0$ and $t_{max}^{-5} = 0$, and solve them for F and v_{core}:

$$v_{core} = \frac{r_0}{t_{core}} = \left(\frac{10E_{ej}(n-5)}{3M_{ej}(n-3)}\right)^{\frac{1}{2}} = \sqrt{\frac{5(n-5)}{3(n-3)}} \cdot \sqrt{\frac{2E_{ej}}{M_{ej}}}\ , \tag{2.11}$$

$$F = \frac{1}{4\pi n} \cdot \frac{(3(n-3)M_{ej})^{\frac{5}{2}}}{(10(n-5)E_{ej})^{\frac{3}{2}}} = \frac{10(n-5)E_{ej}}{4\pi n} \cdot v_{core}^{-5}\ . \tag{2.12}$$

The values of v_{core} and F are not only dependent on the variables occurring in Equation (2.11) and (2.12), but in principle also on the integration boundaries. However, the values for v_{core} and F depend only weakly on these integration boundaries since the assumptions, $t_{min} << t_{core}$ and $t_{max} >> t_{core}$, are satisfied most of the time.

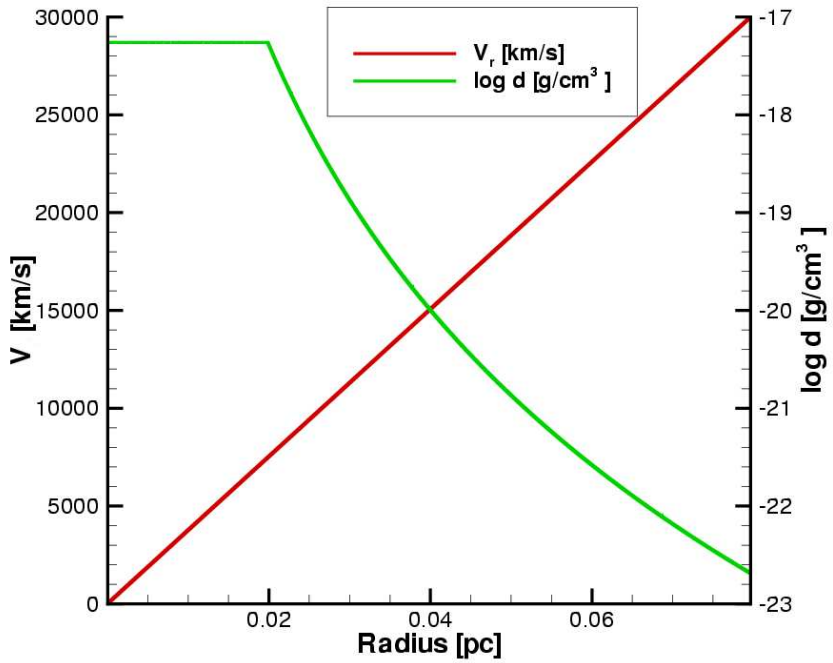

Figure 2.1: An example of the radial density and velocity profile of supernova ejecta at a fixed time. The free expansion of the ejecta can be seen in the velocity profile which is linear with radius. The density profile matches equation 2.5.

Figure 2.1 shows an example of the radial density and velocity profile at a fixed time. Since ZEUS3D is not capable of handling relativistic effects the maximum velocity could not be chosen equal to the velocity of light. We chose an arbitrary maximum velocity of 30000 km/s. Because the drop in density is very strong at high velocities, the choice of a higher maximum velocity will not have a large influence on the hydrodynamical evolution.

2.4 Clumping of the Supernova Ejecta

Kifonidis et al. (2003) have shown that the structure of core collapse supernova ejecta can be aspherical due to the violent processes inside the star. Besides the asphericity they found, it was also found that at some places the heavier elements could end up in front of the lighter ones. The standard model for stellar structure at the end of the life of a star is the onion skin model, as described in Chapter 1. If heavier elements are found outside lighter ones, it means that some parts of the supernova ejecta would have higher velocities than their surroundings. These features can also be observed in some supernovae remnants (Ghavamian et al. 2005; Winkler & Kirshner 1985)

The structure of the ejecta assumed in Section 2.3 is spherically symmetric. To see what the effect of aspherical ejecta would be, clumps were added in some of our simulations. These clumps are small parts inside the ejecta with a higher density. The density of these clumps was increased by a large factor (500). To keep the clump as intact as possible during the evolution, the entire clump was given the same velocity and the pressure was kept constant with respect to the surrounding medium.

Although the observations show that the clumps in some SNR have a higher velocity than their surroundings we did not increase the velocity of our clumps. This was done for simplicity. To get a realistic idea of the effect of clumping one would have to use the results of core collapse simulations.

2.5 Ejecta-CSM interaction

When simulating the interaction of a stellar wind with the CSM we let this stellar wind flow into the CSM. When simulating the interaction of the supernova ejecta with the CSM we let the CSM flow into the supernova ejecta. The latter was done by expanding our grid and using the outer boundary of our grid, which is expanding, as inflow boundary. The inflowing matter at the outer boundary of the grid is the CSM. The values for the density, velocity and temperature of the inflowing CSM were calculated with help of the CSM structure obtained from the simulation of the pre-supernova evolution of the CSM. Every time step the grid is enlarged and the CSM

may flow into the new part of the grid. The expansion of the grid is coupled to the velocity of the matter in the grid at that moment.

This method has a big advantage over the method used for the interaction of stellar winds with the CSM, namely the optimal resolution at all times during the simulation. During the simulation the total number of grid cells is kept constant. This means that when the grid expands the resolution decreases. When using grid expansion, the minimum resolution of the grid is equal to the resolution at the end of the simulation. If no grid expansion is used, the resolution of the grid would have been constant. The resolution of a simulation *with* grid expansion is equal to the resolution of a simulation *without* grid expansion only at the end of the simulations. At every other time the resolution of the grid *with* grid expansion is higher.

At the start of the simulation a part of the CSM, which is going to be included in the simulation, is not yet in the current grid. The part which is not yet in the grid is added when the grid expands. This has the disadvantage that one could miss some of the hydrodynamics taking place in that part of the CSM which is not yet in the grid. Since we are simulating supernovae, the time scales in the current grid are very small compared to the time scales in the CSM which is not yet in the current grid. This means that we can safely assume that the hydrodynamical evolution taking place in those parts of the CSM which are not yet in the grid are negligible.

Chapter 3

SN2001em

We wanted to test if the detailed hydrodynamical results for the method we used for the interaction of the supernova ejecta with the CSM would give results which could be compared with the results from different methods. To do this we took a model which was used to reproduce the observations from a supernova remnant with help of different method, and tried if we could do the same but then with the hydrodynamical method. Afterward we also compared our results with the observations.

3.1 The Observations

The Supernova 2001em was discovered on September 20 2001, by Papenkova et al. (2001), who argued that the explosion date was the 10th of September 2001. The explosion date has a five day uncertainty. The distance to the host galaxy is 84 Mpc. Within a three year period, the supernova was rediscovered because of a rebrightening in the radio and X-ray regime (Stockdale et al. 2004; Pooley & Lewin 2004; Stockdale et al. 2005). The high radio and X-ray flux observed was unprecedented for a supernova at that age. At day 970 an Hα emission line was observed with a Full Width at Half Maximum (FWHM) of approximately 1800 km/s (Soderberg et al. 2004). The results described below show an attempt to reproduce the observations with help of a model, describing the evolution of the progenitor star and the ejecta mass and energy for the supernova explosion, taken from Chugai & Chevalier (2006).

3.2 The Model

Two models were initially proposed, trying to explain the high X-ray and radio fluxes at late times in the evolution of SN 2001em. The first one is a misaligned jet model, the second is a model describing the interaction of

the supernova ejecta with a high density circumstellar shell. A comparison between the two models can be found in Granot & Ramirez-Ruiz (2004).

The model adopted here consists of a star which went through a RSG phase with a very high mass loss which resulted in a high density CSM. After that the star went through a short WR phase which lasted for 1310 years. During the WR phase the stellar wind swept up a large portion of the mass and accumulated it in a shell, the WR shell, at some distance ($\sim$0.02 pc) to the central star. The parameters used for the stellar mass loss in the model here can be seen in Table 3.1. These are the same parameters as used in a model proposed by Chugai & Chevalier (2006), CC06.

CC06 assumed a structure for the CSM prior to the supernova explosion, and with help of the thin shell approximation, as described in Chevalier (1982), they treated the interaction of the supernova ejecta with the CSM. The observations of the supernova were used to constrain the density structure of the CSM prior to the supernova explosion and the model for the progenitor evolution was chosen in such a way that it would explain this CSM density structure.

Their conclusion was that the proposed model for the interaction of the supernova ejecta with a dense shell in the CSM could reproduce the observed X-ray and radio luminosities. However, the evolution of the progenitor was uncertain. The high mass loss rate during the RSG phase was probably the result of a common envelope phase of a binary, in which the envelope of the exploding star was expelled. This also explains the short time in which the high mass loss occurred.

Table 3.1: Assumed wind parameters for our model of the progenitor star of SN 2001em. The table shows the mass loss rate, wind velocity and duration of the phases. The last two columns give the total amount of mass and kinetic energy deposited into the CSM during these phases.

	$\dot{M}[M_\odot/yr]$	$v[km/s]$	$t[yr]$	$\Delta M[M_\odot]$	$\Delta E[10^{45}erg]$
Red Super Giant	10^{-2}	10	260	2.6	5.17
Wolf Rayet	10^{-5}	10^3	1310	0.0131	260.6

3.3 Results

3.3.1 Pre-supernova CSM Evolution

The evolution of the density structure in our model for the CSM of the progenitor star of SN 2001em is shown in Figure 3.1. A spherical coordinate system was used in this simulation with 1000 radial grid points and 200 grid

points in the ϕ-direction. The maximum size of the grid was 0.05 pc in the radial direction and the φ-direction was set to range from 0 to 45^o. This means that the line of sight in the figures showing the structure of the CSM is the polar axis of the star.

The figure shows, from left to right, four snapshots in this evolution at 240, 550, 870 and 1570 years after the start of the RSG phase. The leftmost snapshot is just before the start of the WR phase. The last one is at the end of the WR phase, which is used as input for the supernova calculation. Figure 3.3 shows the angle averaged density distribution of the last part of Figure 3.1. Figure 3.3 shows a density jump of approximately a factor of 1000 at 0.02 pc. The total amount of mass in the grid at the end of the WR phase is $2M_{\odot}$. This is less than the total amount of mass that is lost during both the RSG and WR phases, because a part of the mass lost during these phases has passed the outer boundary of the grid.

In the last slice of Figure 3.1, we can see the hot bubble of the WR wind. This starts at a radius of approximately 0.014 pc and ends at the high density jump at a radius of 0.02 pc. This part of the CSM is very hot and has a high pressure.

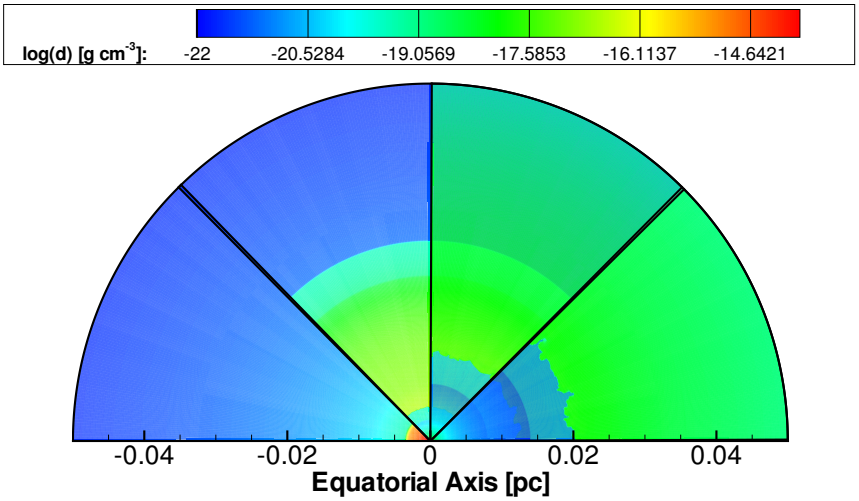

Figure 3.1: Evolution of the CSM density structure prior to the supernova explosion. From left to right it shows, on a logarithmic scale, the density at 240, 550, 870 and 1570 years after the start of the RSG phase. The color coding is given by the colorbar above the figure.

Comparing our result with the model from CC06, which is shown in Figure 3.2, we do not have a single thin shell, but a very thick shell with a high density. The fact that we do not have the single high density shell, as assumed in the CC06 model, is due to the ionization during the WR phase.

At the start of the WR phase the entire grid is ionized and this sets the minimum temperature to 10^4 K, which increases the internal pressure and expands the swept up mass by the WR wind, which would otherwise have been a thin shell, similar to the shell in the CC06 model. The expansion is so high that the outside of the WR shell has moved outside the grid in the third and fourth slice of Figure 3.1. This means that a part of the mass which was lost during the RSG phase has moved out of the grid, this can be seen by the difference in the amount of mass lost and the total amount of mass in the grid.

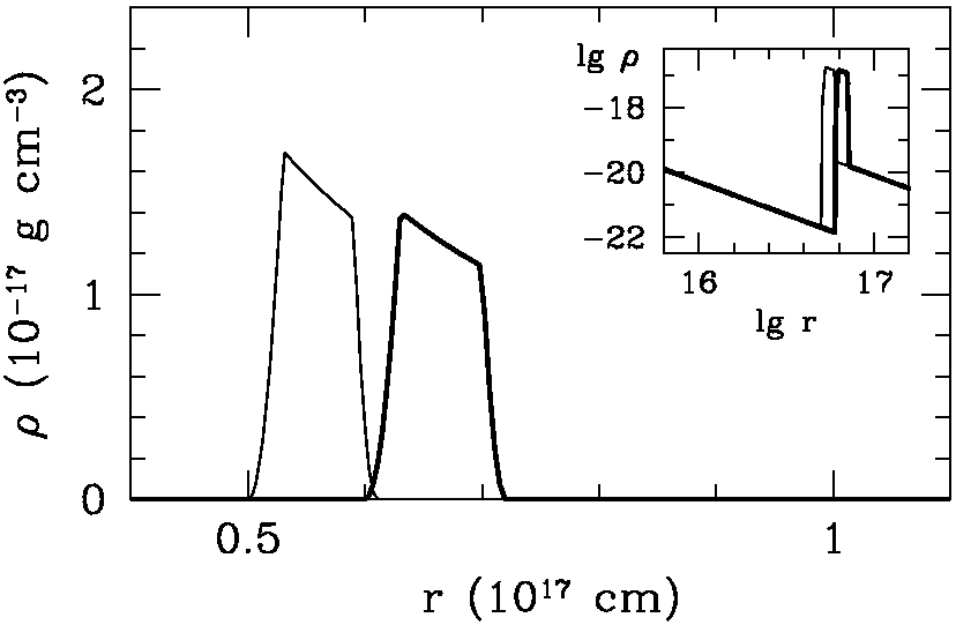

Figure 3.2: Figure from CC06 showing the assumed CSM density structure for the two models A(thick line) and B (thin line). Two high density shells at a different radii are assumed. The inlay shows the same figure but with a logarithmic r and ρ axis.

The density in our shell is around 10^{-18} g cm^{-3}, which is one order of magnitude lower than the density in the shell of CC06. This is not surprising if one takes into account the effect of the expanding shell due to ionization, which was not done in the assumed CSM density structure of the model from CC06.

The difference between the two dimensional CSM density structure and the angular average is not large. Nevertheless there is more structure in the two dimensional case which will affect the evolution of the SNR. This will become clear in the next section.

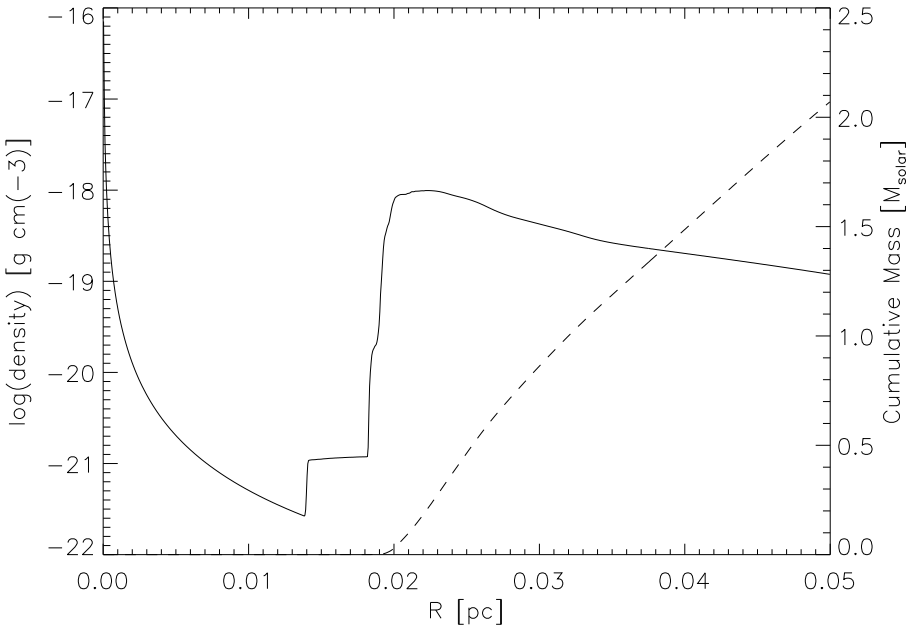

Figure 3.3: Angular average of the two dimensional CSM density structure which is used as input for the supernova simulation. The solid line shows the density and the dashed line shows the cumulative mass.

3.3.2 The Supernova

Figures 3.4 and 3.5 show the initial ejecta properties for the simulation of SN 2001em. The outer edge of the ejecta is located at 0.0008 pc, which shows as a jump in density and velocity in the corresponding figures.

As can be seen in Figure 3.4, clumps were added in this simulation. These clumps have a density contrast of a factor of 500 with their surroundings. The velocity inside the clumps is the same throughout the entire clump, to make sure that they stay as intact as possible.

Only one half of the grid, in the angular direction, is used to add clumps to the supernova ejecta. This has been implemented on purpose, to see the effects of clumping on the SNR evolution in comparison to the evolution of the SNR without clumping. Figures 3.6 and 3.7 show the density and radiative energy loss for SN 2001em at approximately 950 days after the initial explosion, which is approximately the time of the observations of the late time high radio and X-ray flux.

Figure 3.6 shows a very clear effect of the clumps. Two of the clumps initially set in the supernova ejecta did not get destroyed and are now moving into the CSM. These two clumps were initially at the smallest radial distance

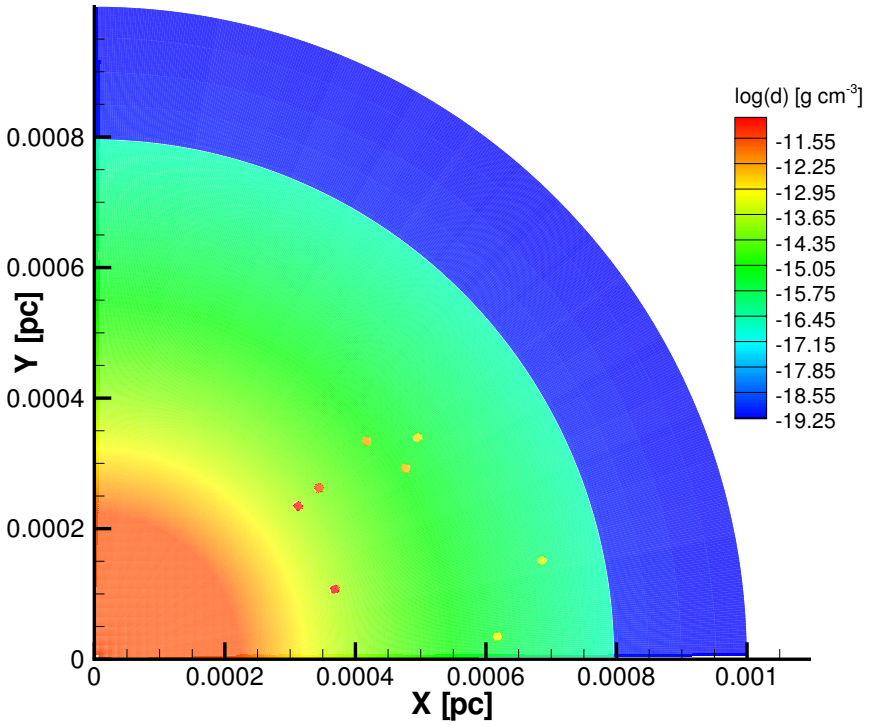

Figure 3.4: The initial supernova ejecta density structure for our simulation of SN 2001em. The color bar in the figure indicates the corresponding values for the density, on a logarithmic scale.

from the center. They were not destroyed because they were the last to collide with the high density jump. The forward shock already accelerated the matter at this density jump and this made it easier for the clumps to overcome the density barrier. Would the velocity of the clumps be enhanced, they would have collided with the unaccelerated matter, at the density jump. If this would have happened the clumps would probably dissolve in the matter with which they collided, in a similar way in which this has happened with the clumps in the results shown here. The result of the clumps is that the radius of the forward shock at the position of the clumps is now larger than at other places, where there were no clumps. The clumps also create a bow shock behind them, and within the region set out by these bow shock there are large difference in the density, up to 2 orders of magnitude approximately.

The region between the forward and reverse shock is the main contributor

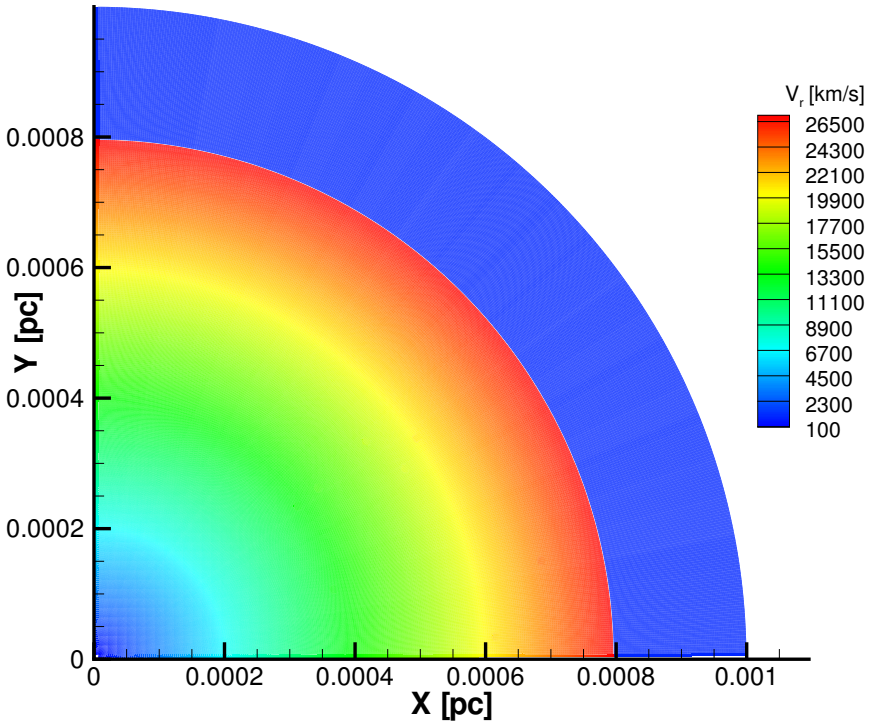

Figure 3.5: The initial supernova ejecta velocity structure for our simulation of SN 2001em. The color bar in the figure indicates the corresponding values for the velocity.

to the radiative energy loss. The increase in energy loss outside the forward shock is an effect of the method used to simulate the supernova ejecta. That part of the CSM has only just entered the grid, and the radiative cooling only applies to those parts of the CSM which are in the grid. The energy lost there should thus have been lost a long time ago already. However, the amount of energy lost in this region is negligible compared to the region within the shocks, so no adjustments have to be made.

Figure 3.8 shows the bolometric and X-ray light curves for our model of SN 2001em. The bottom graph shows the bolometric light curve and the upper one the X-ray light curve. This X-ray curve has been made by assuming that all the radiative energy loss is emitted through thermal radiation. This assumptions excludes non-thermal processes like synchrotron radiation. The same assumption was also made in CC06, in which the X-ray luminosity was calculated only using a bremsstrahlung cooling function.

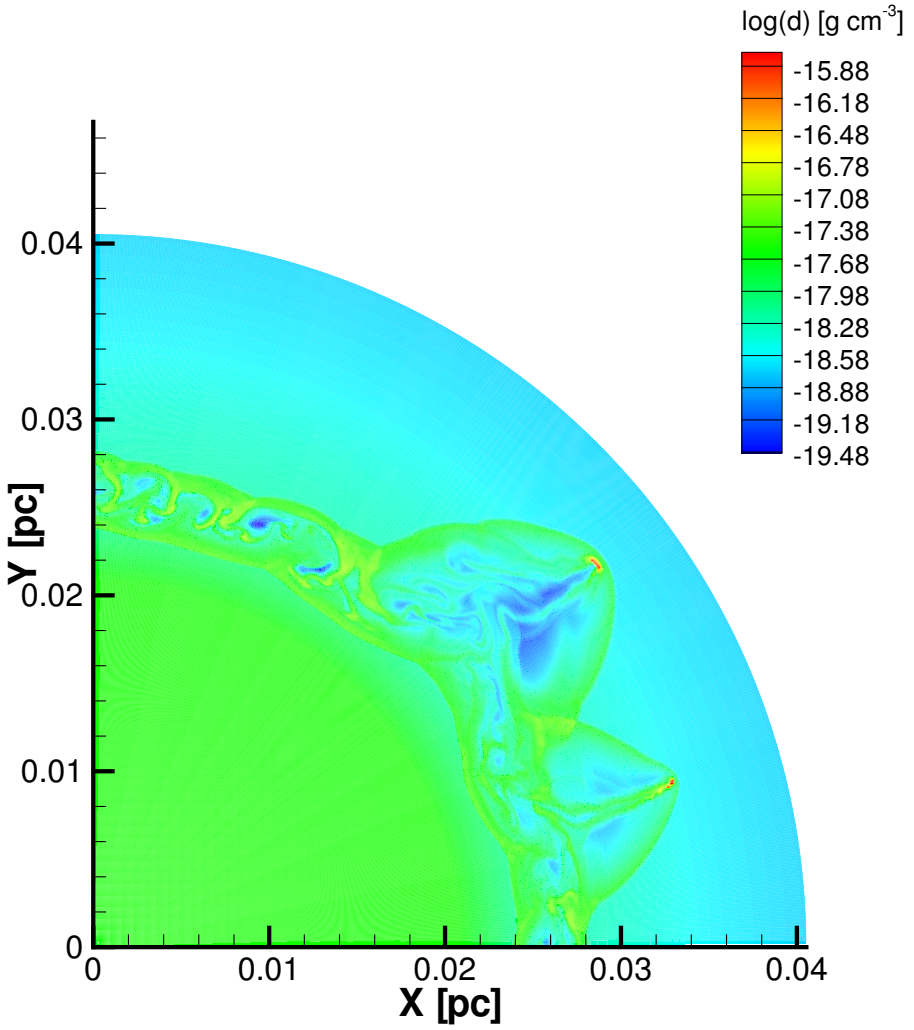

Figure 3.6: The density structure for the SNR at approximately 950 days after the explosion. The color bar in the figures shows the values for the density, on a logarithmic scale, corresponding to the colors.

With the assumption of thermal radiation and the choice of several temperature ranges, which due to the assumption of thermal radiation correspond to wavelength ranges, one can put the radiative energy loss of every grid cell into a certain wavelength range. The temperature range used to determine the the X-ray emission is shown in the graph. The amount of shocked mass, which also falls within a specific temperature range, determines the height of the X-ray luminosity, and since the amount of shocked mass increases, the luminosity increases. The decrease in the X-ray light curve

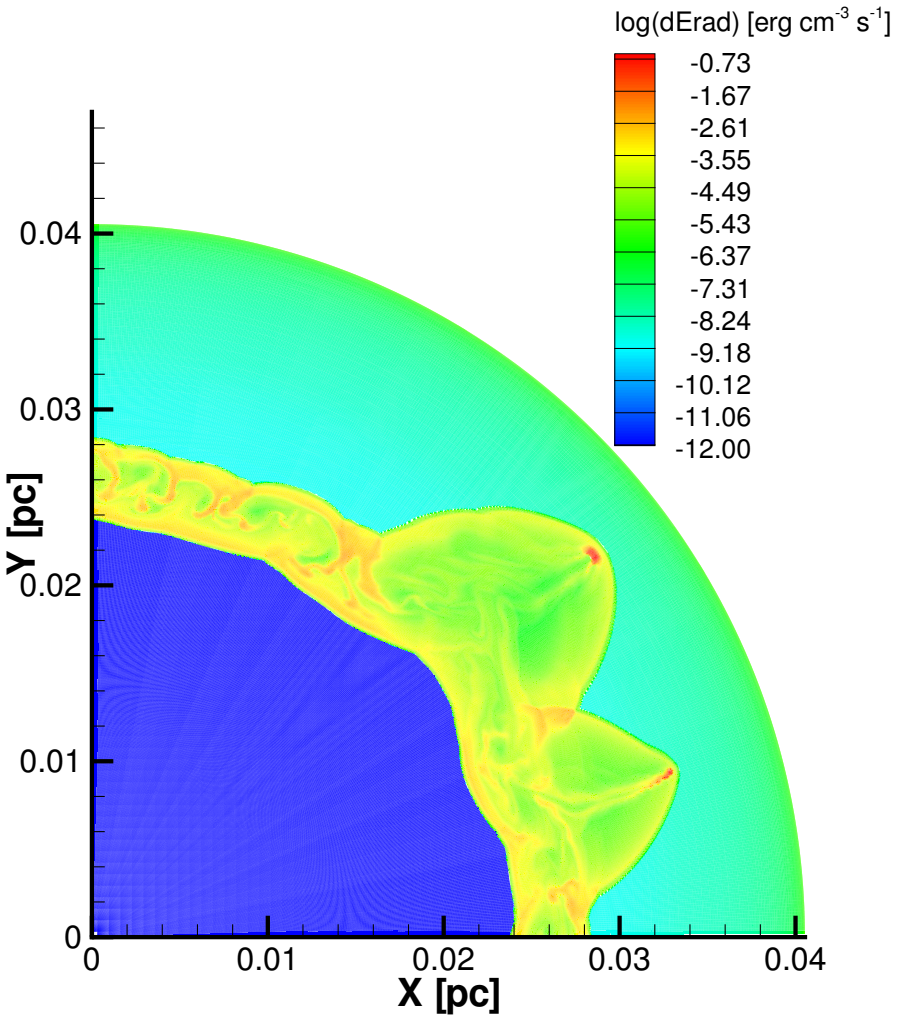

Figure 3.7: The radiative energy loss structure for the SNR 950 days after the explosion. The color bar shows which color corresponds to which amount of radiative energy loss. The colorbar has been set to a minimum of 10^{-12} erg cm^{-3} s^{-1} to get a reasonable contrast within the figure. The actual radiative energy lost in the region within the reverse shock (at 0.024 pc) is even lower than that value, because that part of the grid has already cooled down to 100 K and cannot lose any more energy through radiation.

Above the two figures are numbers for the total energy lost during the time shown in the figure. In the bottom figure this corresponds to all the energy lost through radiation and in the top figure this is the energy lost only in the X-ray regime. As can be seen the radiative energy loss is dominated

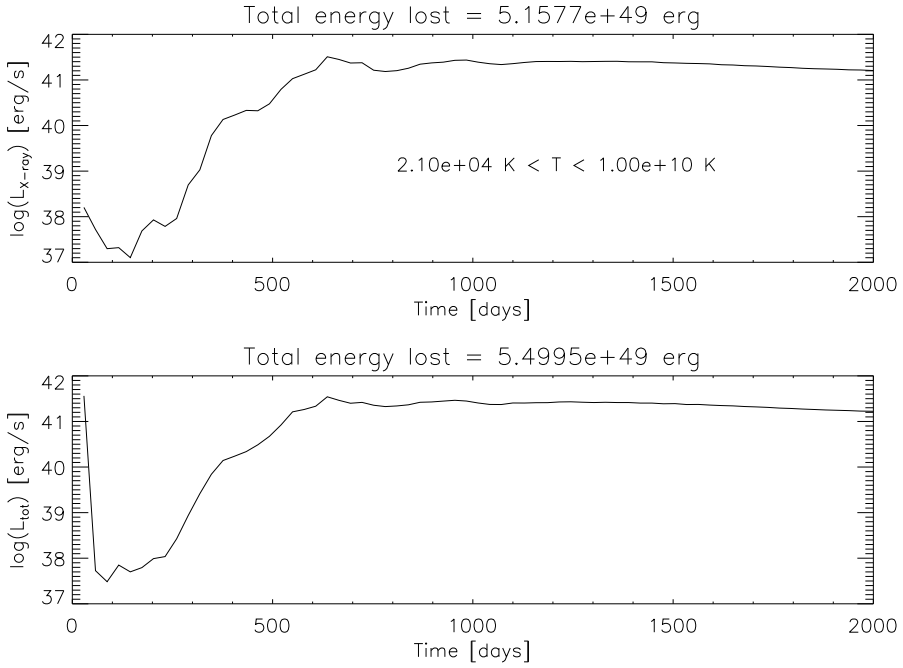

Figure 3.8: Light curves for our model of SN 2001em. The bottom graph shows the bolometric light curve and the top one the X-ray light curve. The X-ray light curve was made by assuming that the radiative energy loss, was all thermal radiation, which means that one can link a temperature to a wavelength regime. The temperature range which was used to calculate the X-ray light curve is indicated in the figure. The number for the total amount of energy lost correspond to the energy lost in the period shown in the figure, either in the X-ray regime or the amount of energy lost through radiation in general.

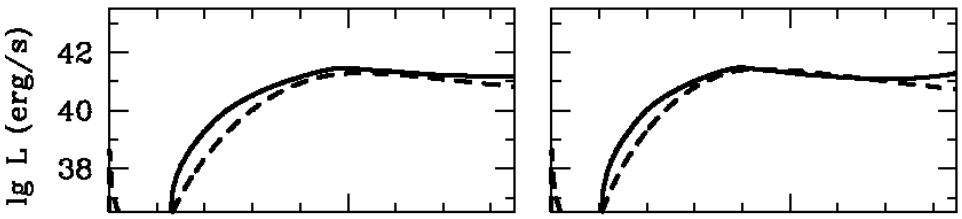

Figure 3.9: Figure from CC06 showing the unabsorbed X-ray luminosities at the forward (solid) and reverse shock (dashed). The tick marks on the x-axis each correspond to 200 years, starting from 0. The large tick mark thus indicates 1000 year.

by the X-ray radiation. Since almost all the radiation is coming from the region between the shocks and this region is very hot, this is not surprising.

Figure 3.9 shows the X-ray light curves from the results of CC06. Here it can be seen that the difference in model A and B, does not have a large effect on the unabsorbed X-ray luminosity, although the difference in shell mass for instance is 25%. The height and rise time of the X-ray light curves is similar to the X-ray light curves from our result. The X-ray luminosity in our result at t=937 days is equal to $2.5 \cdot 10^{41}$ erg which corresponds nicely to the observed value at that time. The peak in the bolometric luminosity at early times is due to the cooling of the ejecta. Although the cooling of the ejecta is dominated by adiabatic cooling, since it is expanding so fast, the ejecta also cools through emitting radiation and because there is a high amount of mass in the supernova ejecta the increase in luminosity remains visible.

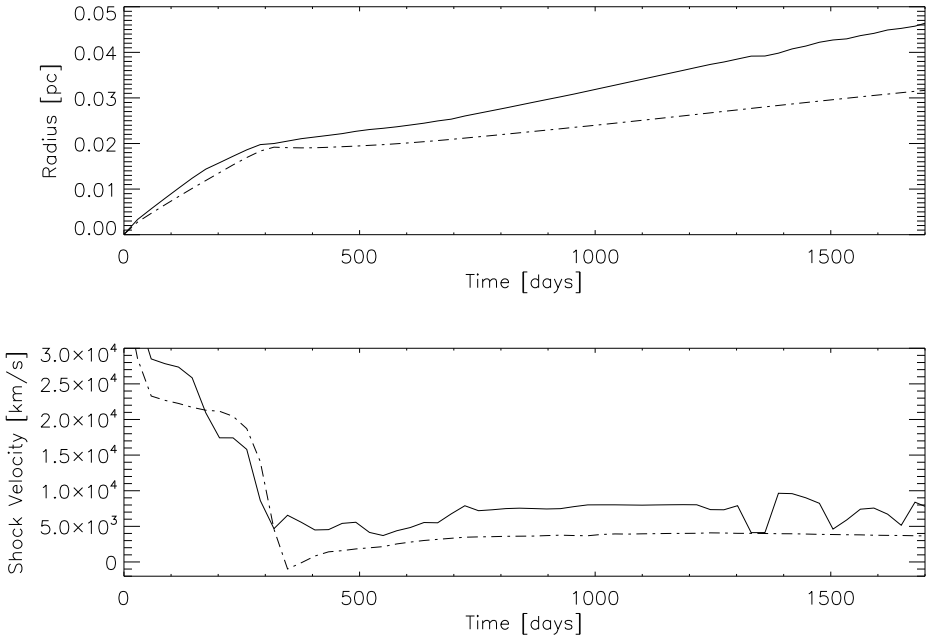

Figure 3.10: Position and velocity of the forward (solid) and reverse (dashed) shock in our model of SN 2001em measured starting from the supernova explosion.

Figure 3.10 shows positions and velocities of the forward and reverse shock in the evolution of our model of SN 2001em. As can be seen the expansion of the forward shock decreases strongly around 250 days after the supernova explosion. This is caused by the interaction of the supernova ejecta with the high density region located at 0.02 pc. Since there is still

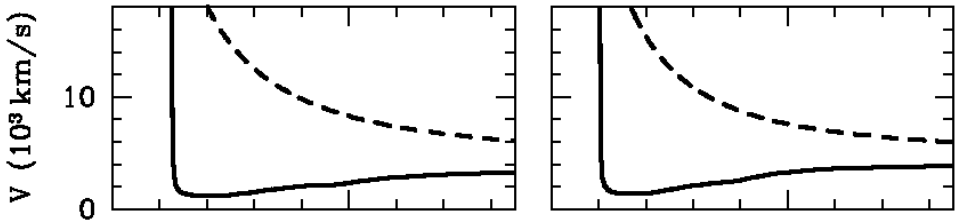

Figure 3.11: Figure taken from CC06 showing the velocity of the thin shell (solid line) and the velocity of the ejecta at the reverse shock (dashed line). The left box corresponds to model A and the right box to model B. The tick marks on the x-axis correspond to a time of 200 days each, starting from 0. The large tick mark thus indicates 1000 days.

supernova ejecta colliding with the shell after 300 days the forward and reverse shock accelerate again.

Figure 3.11 shows the velocity of the thin shell and the velocity of the ejecta at the reverse shock for the results from CC06. The velocity of the thin shell should correspond to our forward shock velocity. Since we did not have a thin high density shell, the collision of the supernova ejecta resulted in a forward shock with a higher velocity. In our results the velocity of the forward shock at 950 days is 8000 km/s and in the results from CC06 it is approximately 2000 km/s. The velocity of the forward shock might thus be an indicator of the mass which has been swept up in the shell.
Figure 3.12 shows the velocity structure of the SNR 950 days after the explosion. The part between the forward shock and the reverse shock is thought to be the origin of the matter which is emitting the Hα radiation. The FWHM of the observed Hα line was 1800 km/s per second. The average velocity of the matter in this region in our model is approximately 6000 km/s, which lies well above this 1800 km/s. Although there are some parts which do have velocities corresponding to this FWHM. If we would have had a single high density shell, as in CC06, the acceleration of the matter would have been slower, and the velocity of the matter between the forward and reverse might have been corresponding better with the observed FWHM of the Hα radiation. This explains why CC06 were able to reproduce the FWHM of the observed Hα line.

3.4 Conclusions

We simulated the pre-supernova evolution of the CSM and the interaction of the supernova eject with the CSM, based on a model taken from CC06. We were not able to reproduce the CSM density structure of CC06 through hydrodynamical simulations, since the inclusion of ionization inhibited the

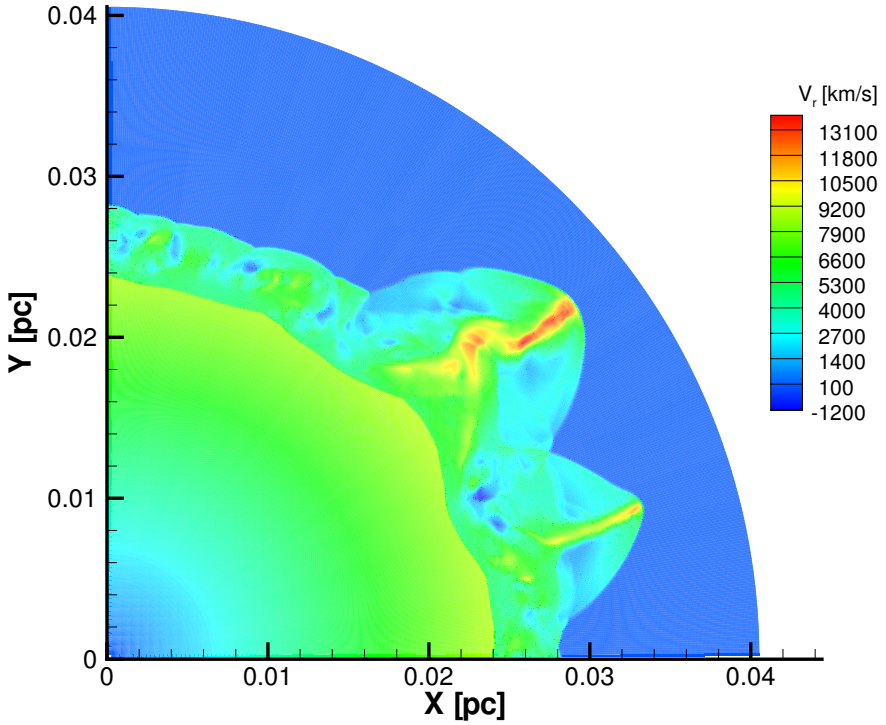

Figure 3.12: The SNR velocity structure 950 days after the explosion. The colorbar in the figure indicates which velocity belongs to which color.

formation a thin WR shell. Instead our result showed a thick WR shell, with a lower density than the thin shell in CC06.

In the method from CC06 and our method, for the interaction of the supernova ejecta with the CSM, the start of the rise of the X-ray luminosity occurs at the same time. Since the high density jumps in the pre-supernova structure for the CSM for our result and those of CC06 was the same, this is no surprise. The height and rise time of the X-ray luminosities in both methods are similar. The total amount of shocked mass and the temperature of that shocked mass determine the X-ray luminosity of the SNR at a given point in time. Since the total amount of shocked mass in our result is lower than that in the results of CC06, the fact that the X-ray light curves look similar is surprising. However, the differences in the models A and B from CC06 do not result in a large difference in the X-ray light curves for those models. This suggests that the height of the X-ray light curve is not strongly dependent on for instance the circumstellar shell mass. In our result the total

amount of mass is even lower but still the light curves look similar, which strengthens the suggestion of the weak dependence.

The difference in the velocity of our forward shock compared to the velocity of the thin shell in the results from CC06 can be attributed to the different structures of the CSM. Because the density jump at the WR shell was smaller in our results than in those of CC06, our forward shock had a higher velocity. The velocity of the matter between the forward shock and the reverse shock was also higher in our results than in the case of CC06. This matter is thought to be the origin of the Hα radiation. The difference in velocities is caused by the difference in the pre-supernova CSM structure. In our results the lower density of the WR shell caused higher velocities. It is interesting that the FWHM of Hα radiation can perhaps be used as an indicator of the density of the CSM, since it is the result of the shocked CSM material. Increasing the density of the CSM would then result in a lower FWHM of the observed Hα line.

Comparing our results with the observations we see that we do produce an X-ray luminosity corresponding to the observed value at the right time after the supernova explosion. The FWHM of 1800 km/s is however not reproduced. This might however be solved by changing the progenitor evolution in such a way that the density of the CSM is higher.

Given the similarities, and explained differences, of the results from our model with the results from CC06, we conclude that the method we are using for treating the supernova ejecta is producing results that can be used.

To be able to compare the results of our simulation with the observations better, it would be useful to have more data concerning the X-ray luminosity at different times. The results predict that the high X-ray luminosity will remain high until 1700 days after the explosion. More observations of the SNR could check this prediction.

Chapter 4

Cassiopeia A

The Cas A supernova remnant has long been a subject of study. To this day the progenitor evolution of the Cas A remnant is not well known. In this chapter we present an analysis of two progenitor evolution models, of which one was tested to see if it could reproduce some of the observations of Cas A. Both the pre-supernova evolution of the CSM and the supernova ejecta interacting with this CSM were computed.

4.1 Observations

Cas A is a galactic SNR at a distance of $3.4^{+0.3}_{-0.1}$ kpc (Reed et al. 1995). Thorstensen et al. (2001) calculated an age of approximately 325 years, by using the proper motion of ejecta knots. Gotthelf et al. (2001) determined that the position of the forward shock of the remnant lies at 2'.55 ± 0'.2 (2.55 ± 0.2 pc) and the reverse shock 1'.58 ± 0'.16 (1.58 ± 0.16 pc).

In the optical the SNR consists of, among other things, Fast Moving Knots (FMK), which are moving at velocities around 10000 km/s and slower moving knots, also known as Quasi Stationary Flocculi (QSF), which move with velocities below 500 km/s (Fesen et al. 2001). The FMK are part of the supernova ejecta. The lack of hydrogen rich material in Cas A suggests that it was a WR star when it exploded (Woosley et al. 1993). The QSF emit Hα radiation indicating that the QSF are likely a part of a hydrogen rich stellar envelope, ejected in a stellar wind prior to the supernova explosion. This explanation for the origin of the FMK and the QSF has been already proposed by van den Bergh (1971). The total amount of mass swept up by the forward shock is about 8 $M_{\odot}$ (Vink et al. 1996). According to Chevalier & Oishi (2003) the forward shock is now moving into a medium which is consistent with a free streaming RSG wind.

Furthermore the global morphology of Cas A exhibits an asymmetry. This asymmetry seems to arise from an asymmetric supernova explosion as opposed to an asymmetric CSM (Vink 2004). While modeling Cas A,

reproducing this asymmetry has not been our aim.

There have been observations of the compact remnant of the progenitor (Tananbaum 1999; Mereghetti et al. 2002). Following on these observations Young et al. (2006) concluded that the mass of this compact remnant is approximately $2M_{\odot}$.

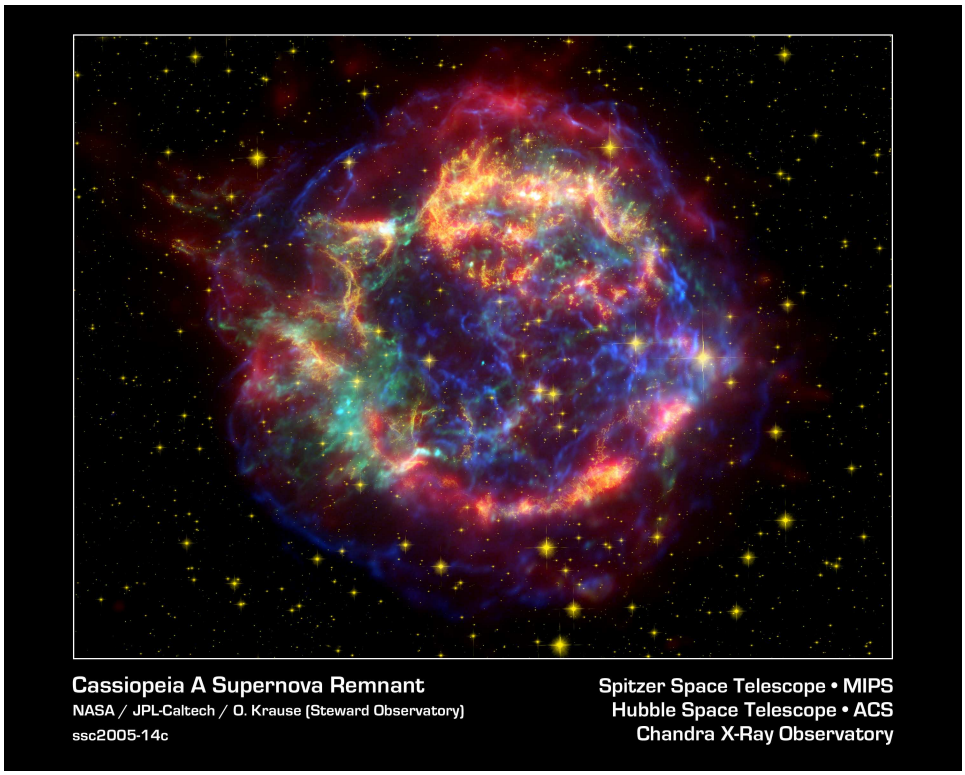

Figure 4.1: Image of the Cassiopeia A supernova remnant. The colors yellow, red, blue and green correspond to broadband spectra of optical, infrared, X-ray and to intermediate energy X-ray, respectively. The image spans approximately 5' by 9'. Image credits: NASA/JPL

4.2 Models for the progenitor of Cas A

4.2.1 Single star or Binary star progenitor

We consider two models for the progenitor of the Cas A SNR. These are the single star model and the binary model. For both of these models the observational constraints mentioned in Section 4.1 have to be satisfied.

The constraint of the forward shock moving into the free streaming RSG wind puts limits on the position of the WR shell at the point of the supernova explosion. The WR shell has to be at a distance from the center of the

supernova explosion which is smaller than the distance of the forward shock in the SNR at this moment in time. In turn this constrains the WR life time of the progenitor star. If the WR life time is too large the WR shell will have moved too far out.

The supernova ejecta mass is approximately 2...4 $M_\odot$ (Vink et al. 1996) and the compact remnant mass is around $2M_\odot$, which means that at the point of the supernova explosion the star had a mass of 4...6 $M_\odot$. This together with the short WR life time constrains the initial mass of the exploding star to about 15...20 $M_\odot$.

4.2.1.1 A binary model

In a binary there are two stars which orbit around each other. Due to normal stellar evolution one of the stars can grow. If the radius of the expanding star grows enough it is possible that the smaller star ends up in the envelope of the larger star, which is called a common envelope phase. Due to the presence of the smaller star in the envelope of the larger star this envelope can get ejected entirely. If the mass is lost in this manner there would be a large asymmetry in the distribution of the lost mass, the majority of which would be close to the orbital plane (Yorke et al. 1995). Such an asymmetry has not been observed in Cas A.

The point in time, during the evolution of the binary system, when the common envelope phase needs to occur is after the core helium burning phase of the star which will lose its envelope. This is called Case C evolution. For a review on Case C, binary and common envelope evolution see Iben & Livio (1993). If the star loses its envelope at that point in time, it has only a short amount of time to live thereafter. During this time the star will be a WR star, which means that the star will only have a short WR phase, as required by the observations. This binary model thus naturally provides a short WR life time.

However, the probability that a binary system ends up in a common envelope phase at the right time in the evolution is small. The radius of the envelope losing star will have to be larger at that specific time than it has ever been before. If this is not the case, the common envelope phase of the binary would have occured earlier in the evolution. This would mean the star has a much longer WR life time, which would contradict the fact that the forward shock is currently running into a free streaming RSG wind.

The interaction of the WR wind with the mass lost during the previous mass loss period will create a high density shell around the binary system. This shell will be subject to Rayleigh-Taylor (RT) instabilities, because he low density WR wind is accelerating the high density RSG matter, and will thus be clumpy. These clumps are though to be the origin of the QSF in the Cas A SNR.

4.2.1.2 A single star model

The single star model with a RSG phase and a WR phase will create also a high density shell. The WR wind will sweep up a part of the mass ejected during the RSG phase, and create the high density shell which will be affected by RT instabilities and thus be clumpy.

The fact that the progenitor star evolution is required to end in a WR phase puts constraints on the mass of the star in this model. In Meynet & Maeder (2005) it is shown that stars with a mass as low as $20M_{\odot}$ at the start of their evolution may end up as a WR star. The stars with the lowest initial masses also have the shortest WR life times. If one assumes a short WR life time this immediately takes care of another constraint, being that the forward shock is currently running into a free streaming RSG wind. This is satisfied since the short WR life time makes sure that the WR shell is close enough to the place were the supernova will explode. According to Kwok (2000), the velocity of a shell, which is the result of two winds interacting, can be calculated by:

$$V_s = \left(\frac{\dot{M}_2 V_2^2 V_1}{3\dot{M}_1} \right)^{\frac{1}{3}}. \tag{4.1}$$

Here V_s is the velocity of the shell, $\dot{M}_1$ and V_1 are the mass loss rate and velocity during the first wind and $\dot{M}_2$ and V_2 are the mass loss rate and the velocity of the second wind. Given a mass loss rate and velocity during the RSG phase of $10^{-5} M_{\odot} yr^{-1}$ and 10 km/s, and mass loss rate and velocity during the WR phase of $10^{-5} M_{\odot} yr^{-1}$ and 2000 km/s, the shell velocity will be 237 km/s. If the WR phase lasts 10000 years the radius at which the WR shell will be located is equal to 2.43 pc.

During the RSG phase of the progenitor star, it has to lose its entire envelope, since at the end of the RSG phase the star has to become a WR star. To do this the assumption of an enhanced mass loss rate during the RSG phase has to be made. This enhanced mass loss rate is warranted by the uncertainty there is in RSG mass loss rates. Comparing the description of the RSG mass loss rate from de Jager et al. (1988) and Salasnich et al. (1999), one can see a difference of a factor of 10 in the RSG mass loss rate is not uncommon.

The $20M_{\odot}$ stellar model from Hirschi et al. (2004) shows that the mass of the core at the point of the supernova explosion is approximately $6M_{\odot}$, which is within the range allowed by the supernova ejecta mass and the mass of the compact remnant in Cas A.

4.2.1.3 Conclusion

The main arguments against the binary star progenitor model are the fact that no large scale asymmetry is observed, the total amount of mass that has to be swept up by the forward shock may be too large and the fact that the probability that the binary evolution model would occur is small. An argument in favor of the binary model would be that it naturally produces a short WR life time.

The arguments in favor of the single star model is that it can produce the right masses for the swept up mass by the forward shock and the right amount of ejecta mass. Besides that, the stellar evolution models warrant the choice of a short WR phase for a star of relatively low mass. To conclude, we think it is more likely that the progenitor star of the Cas A SNR was a single star, and thus we chose the single star model to try to reproduce the Cas A SNR.

4.2.2 The adopted model

The stellar evolution model discussed in Hirschi et al. (2004), for a star with an initial mass of 20 $M_{\odot}$, is the one used in this thesis. This model originally does not have a WR phase in the evolution of the star but we assume that the entire envelope is lost by the stellar wind during the RSG phase. After the entire envelope is lost, the resulting star is a WR star. In this specific case it does not matter for the evolution of the core if the star loses its envelope entirely or only partly, which means that we can assume the enhanced mass loss rate without affecting other parameters for the stellar evolution. The parameters used for the adopted model are summarized in Table 4.1.

Table 4.1: Wind parameters for our models of the progenitor star of Cas A. WR 1 and 2 correspond to model 1 and 2. Mass loss rate and velocity during the RSG and WR phases, and the duration of each of these phases. The last two columns give the total amount of mass and kinetic energy deposited into the CSM during these phases.

	$\dot{M}[M_{\odot}/yr]$	$v[km/s]$	$t[yr]$	$\Delta M[M_{\odot}]$	$\Delta E[10^{45}erg]$
Red Super Giant	$1.54 \cdot 10^{-5}$	4.70	$8.75 \cdot 10^{5}$	13.5	5.93
Wolf Rayet 1	$9.72 \cdot 10^{-6}$	$1.716 \cdot 10^{3}$	$1.77 \cdot 10^{4}$	0.17	$1.0 \cdot 10^{4}$
Wolf Rayet 2	$9.72 \cdot 10^{-6}$	$1.716 \cdot 10^{3}$	$1.14 \cdot 10^{4}$	0.11	$6.5 \cdot 10^{3}$

The star has a mass of 19.5 $M_{\odot}$ at the end of the MS and the core of the star has a mass of 6 $M_{\odot}$ at the end of the RSG phase. This means that during the RSG phase 13.5$M_{\odot}$ have to be lost in the stellar wind. The stellar model from Hirschi et al. (2004) gives the RSG lifetime, so combining this with the

total amount of mass that has to be lost, we compute the RSG mass loss rate. The total amount of mass lost during the WR phase is small. The velocity of the wind during the RSG phase was determined by using the amount of swept up mass by the supernova. The total amount of swept up mass is $8M_{\odot}$, which resides within 2.5 pc, so one can integrate the density of the RSG wind, assuming a density profile consistent with a free streaming RSG wind, over that radius and obtain the value for the RSG wind velocity with help of:

$$8M_{\odot} = \int_0^{2.5\mathrm{pc}} 4\pi r^2 \frac{\dot{M}}{4\pi r^2 v} \mathrm{d}r = \frac{\dot{M} \cdot 2.5\mathrm{pc}}{v} \ . \tag{4.2}$$

The RSG shell, which is created by the MS hot bubble pushing to the center and the outflowing RSG wind, is outside the region of interest. This was checked by using equation (22) from Weaver et al. (1977) and the equation for the ram pressure of a stellar wind $P_{ram} = \rho v^2$. At the position of the RSG shell the values for the pressure are equal to one another. Using the parameter for the MS phase of the stellar wind given in Hirschi et al. (2004), a typical MS wind velocity of 1000 km/s, a CSM density of 10^{-23} g cm^{-3} and the parameters for the RG wind given in Table 4.1, we obtain a radius for the RG shell of 19 pc. With this in mind, one can assume a r^{-2} density profile for the wind of the RSG phase, which corresponds to a free streaming RSG wind. Since the structure of the CSM during the RSG phase can be determined with the above mentioned assumptions, it was not necessary to calculate the RSG phase, which saved considerable computing time. The values for the WR mass loss rate and wind velocity are calculated with help of the equations (12), (15), (17) and (22) from Nugis & Lamers (2000). The parameters needed for the calculation of the mass loss rate and velocity of the WR wind are taken from the stellar model of Hirschi et al. (2004).

Since the star at the end of its life has a mass around 6 $M_{\odot}$, we adopt a supernova ejecta mass of 4 $M_{\odot}$. This value is allowed by the range of determined ejecta masses (Vink et al. 1996; Willingale et al. 2003). The ejecta energy is set to $2 \cdot 10^{51}$ erg Vink (2004)

4.3 Results

The only real free parameter we have is the duration of the WR phase. By using the result of the CSM structure evolution from different times we can 'put' the WR shell at a different radii in the CSM. As will become clear in the results of our model for the SNR shown below, this has important effects on the evolution of the SNR, and thus constrains the progenitor evolution. In the following sections we show the results of the simulations when using two different CSM structures. The difference in these two structures results

from the difference in WR life time. In model 1 the WR phase lasted 17700 years and in model 2 the WR phase lasted 11400 years.

For all the results shown in this chapter a spherical coordinate system was used (r,θ,φ), with an assumed symmetry in the θ-direction. The number of grid cell in the radial direction was always equal to 1000. The physical size, in the radial direction, of the grid in the pre-supernova evolution simulations was ranging from 0 to 3 pc, and the grid cells were equally spaced over this size. In the case of the supernova calculations the physical size of the radial grid was enlarged each time step, as described in Section 2.5. For each time step the total number of grid cells was redivided over the grid, which resulted in an equally spaced grid for the radial direction at every time. The number of angular grid points, in the φ direction, was equal to 200 in the case of the pre-supernova evolution simulations, and equal to 400 in the case of the supernova simulations. In all cases the angular grid ranged from 0 to 0.25π and the number of grid cells, in the angular direction, were equally spaced. Due to the choice of coordinate system and symmetry axis, all the lines of sight in the figures which show the structure of the CSM and the structure of the SNR, are the polar axis of the progenitor star.

4.3.1 Pre-supernova CSM evolution

With help of the parameters from Table 4.1 the evolution of the CSM due to the stellar wind was simulated. The result can be seen in Figure 4.2. This figure shows four snapshots of the CSM during the WR phase. The time in each frame is, from left to right, 1900, 6650, 11400 and 17700 years after the start of the WR phase. The RSG phase was not actually simulated since the CSM in which the WR phase would start could be derived with help of the RSG wind parameters, as described in Section 4.2.2. The figure shows that during the WR phase not a stable WR shell will form but a fragmented shell in which there are several small and larger clumps with a higher density than the density in the free streaming RSG wind. This clumping is due to the Rayleigh-Taylor instability, since the low density WR wind is accelerating the mass of a high density RSG wind.

4.3.2 Model 1

The WR life time in Model 1 is equal to 17700 years, the structure of the CSM at this points can be seen in the third part of Figure 4.2. Figure 4.3 shows the result for the CSM density structure 325 years after the supernova explosion, the age at which Cas A is thought to be now.
The positions of the shocks in Figure 4.3 can be seen clearly, with the forward shock around 2.7 pc and the reverse shock around 2.2 pc. The dense clumps in between the shocks is what is left of the clumped WR shell. Since they have been hit by the ejecta, the clumps have been partly stripped of the

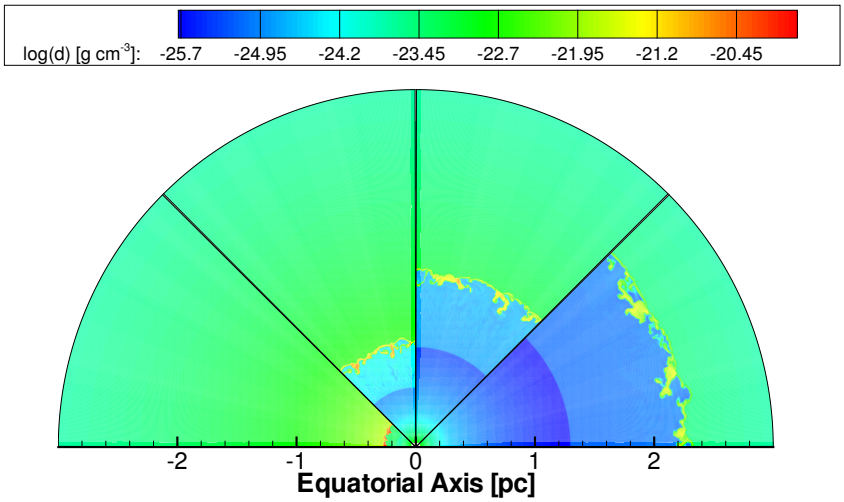

Figure 4.2: From left to right the figure shows the CSM density structure 1900, 6650, 11400 and 17700 years after the start of the WR phase. The color bar above the figure shows the color coding for the density on a logarithmic scale.

mass they contained, and they have been accelerated. The velocities of these dense clumps now ranges from approximately 100 to 1000 km/s. The density of the clumps ranges from $10^{-21.5} \sim 10^{-20.5}$ g cm^{-3}. This can also be seen in Figure 4.4.

This figure shows the mass distribution in the velocity and density plane. In the figure the high density clumps can be seen in the top left. Below the clumps, the product of the collision of the supernova ejecta and the WR shell can be seen as large region in the mass distribution. The unshocked ejecta show as a horizontal line in this figure. Starting from the right end of the unshocked ejecta line, a yellow line, which corresponds to the reverse shock, can be seen. The artificial viscosity smears the shock out over a few grid cells and the values in these cells correspond to the yellow line. The high peak at zero velocity and a density of $10^{-23.7}$ g cm^{-3} corresponds to the outer part of the grid, outside the forward shock, and also exhibits a line which connects it to high mass containing area in the mass distribution, containing the shocked ejecta and shocked CSM. The continuous distribution of mass towards higher velocity and lower density, starting from the highest densities, indicates that these clumps are accelerated by the collision with the supernova ejecta.

The shock positions and velocities are shown in Figure 4.5. The velocity of the shocks is calculated by taking the time derivative of the position of the shocks. The velocity of the forward shock does not change significantly.

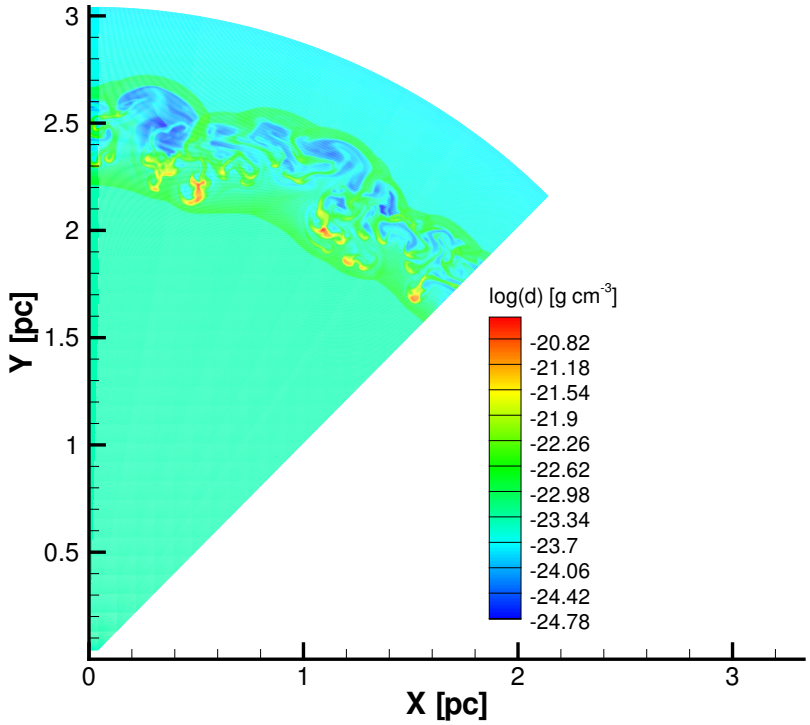

Figure 4.3: Resulting density structure of the SNR of model 1, 325 years after the supernova explosion. The color bar next to the figure shows, on a logarithmic scale, the color coding for the density.

The reverse shock continuously decelerates, which means that in the reference frame of the unshocked ejecta it is moving faster and faster into the unshocked ejecta.

The expansion parameter (δ) of the supernova remnant in our result, which is defined as $R \propto t^{\delta}$, is equal to 0.44. In the Ejecta Dominated (ED) phase of a supernova remnant this is equal to 1, and at the end of the Sedov-Taylor (ST) phase it is equal to 0.4. This means that this supernova is currently at the end of the ST phase, and is going to the pressure driven snowplow phase.

The properties of the Cas A SNR which we think are most important to reproduce are the velocity and position of the forward and reverse shock. This shock structure is not very dependent on the small scale hydrodynamics and will thus not be strongly affected by, for instance, the clumping of the WR shell. It will more strongly depend on parameters which have a influence

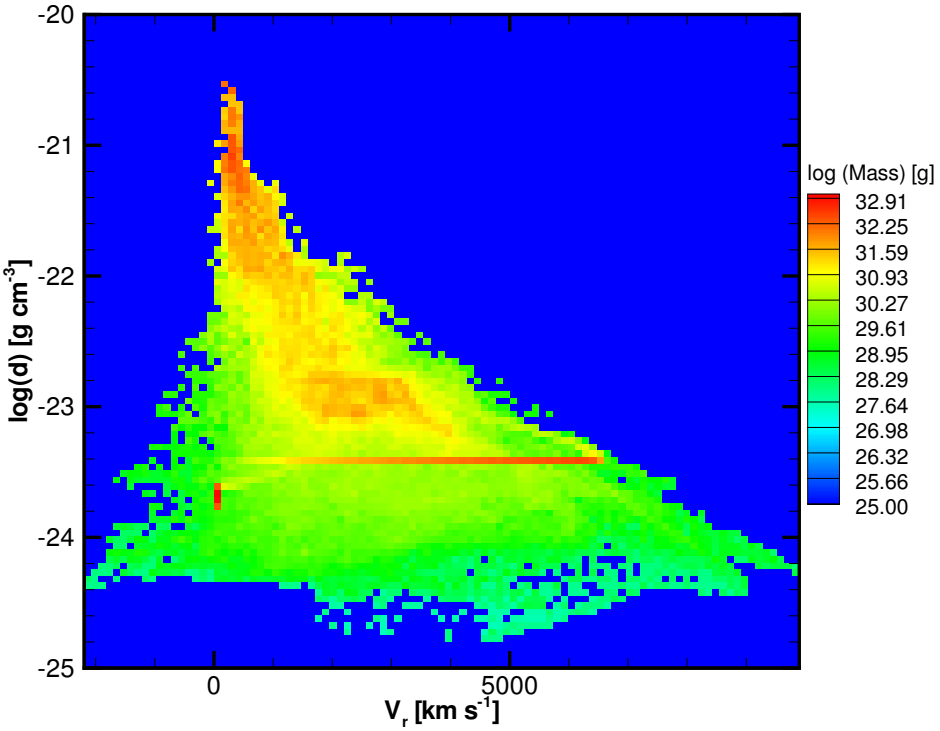

Figure 4.4: Mass distribution showing the amount of mass in a pixel corresponding to a certain range in velocity and density. The colors represent an amount of mass in each pixel, and the corresponding values can be seen in the color bar next to the figure.

on the large scale hydrodynamical structure of the CSM.

The total amount of mass in the WR shell is important in this respect, since the shock needs to pass this shell. If it were larger, or smaller, it would be more difficult, or easier, for the shock to pass it. Since in the model shown above the shock properties are not well reproduced we computed another model. Looking at Figure 4.3 and 4.2, the reverse shock is approximately at the position where the WR shell was at the point of the supernova explosion. Since the observations show the reverse shock to be at a radial distance from the center equal to approximately 1.5 pc we chose the WR life time to be smaller in such a way that the WR shell would be at this radius. This meant that the WR life time was 11400 years in stead of the 17700 years adopted in the above model, and that the mass in the WR shell was less than in model 1.

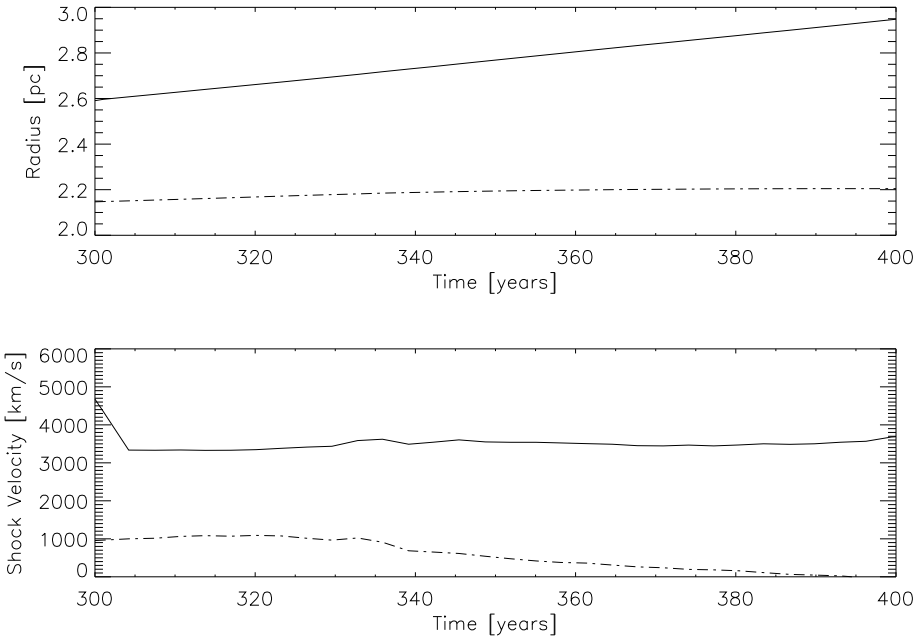

Figure 4.5: Position and velocity of the forward (solid) and reverse shock (dashed) and corresponding velocities for model 1

4.3.3 Model 2

The WR life time in Model 2 is equal to 11400 years, at which time the density structure of the CSM corresponds to the third part of Figure 4.2. Figure 4.6 shows the CSM density structure 325 years after the explosion for model 2. The most apparent feature is again the shock structure. In this case the forward shock can be seen at a radius of 2.5 pc, and the reverse shock at approximately 1.4 pc. The high density clumps around 1.7 pc from the center are the remnant of the instabilities which occured in the WR shell. The density in these clumps ranges from $10^{-21.8} \sim 10^{-21.1}$ g cm^{-3}.

Figure 4.8 shows a mass distribution similar to Figure 4.4, but now containing the data from model 2. The high density clumps can again be seen in the top left part of the figure. The amount of mass which they contain is less if one compares it with the mass distribution from the previous model. This effect comes from the supernova ejecta interacting with the WR shell at an earlier time. Because of this the clumps have been stripped of more mass by the passing supernova ejecta. At the same time the clumps have been accelerated more and this can be seen in the range of velocities which they occupy in the mass distribution. This can be seen in Figure 4.7. Since it is difficult to determine what is a part of the clump and what is not, there is

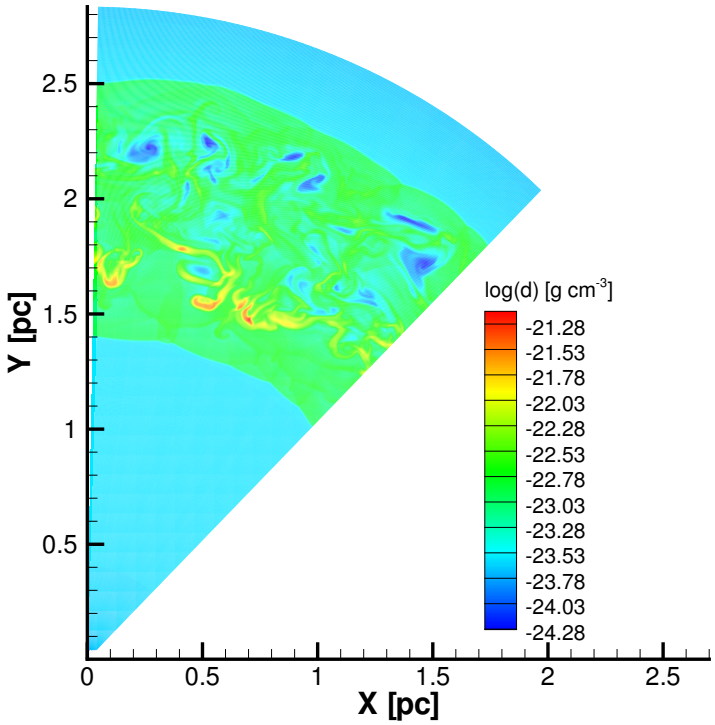

Figure 4.6: Resulting density structure of the SNR of model 2, 325 years after the supernova explosion. The color bar next to the figure shows, on a logarithmic scale, the color coding for the density.

a large range in values for the amount of mass in the clumps. Nevertheless, it can be seen that the general trend is that the mass in the clumps goes down with time and the velocity goes up, as described above.

In Figure 4.8 a strict boundary of allowed densities for the velocities below approximately ∼1000 km/s can be seen. The collision of the forward shock with the WR shell is the cause of this boundary. The pieces of the WR shell which were in this part of the mass distribution were either accelerated by the forward shock or destroyed by it. The unshocked part of the ejecta can again be seen as a horizontal line. The unshocked supernova ejecta extend to higher velocities in Figure 4.4 than in Figure 4.8. This is caused by the location of the reverse shock. In Model 1 the reverse shock is at a larger radius from the center than in Model 2, which means that the still freely expanding supernova ejecta have higher velocities in Model 1, since they have not been decelerated by the reverse shock yet.

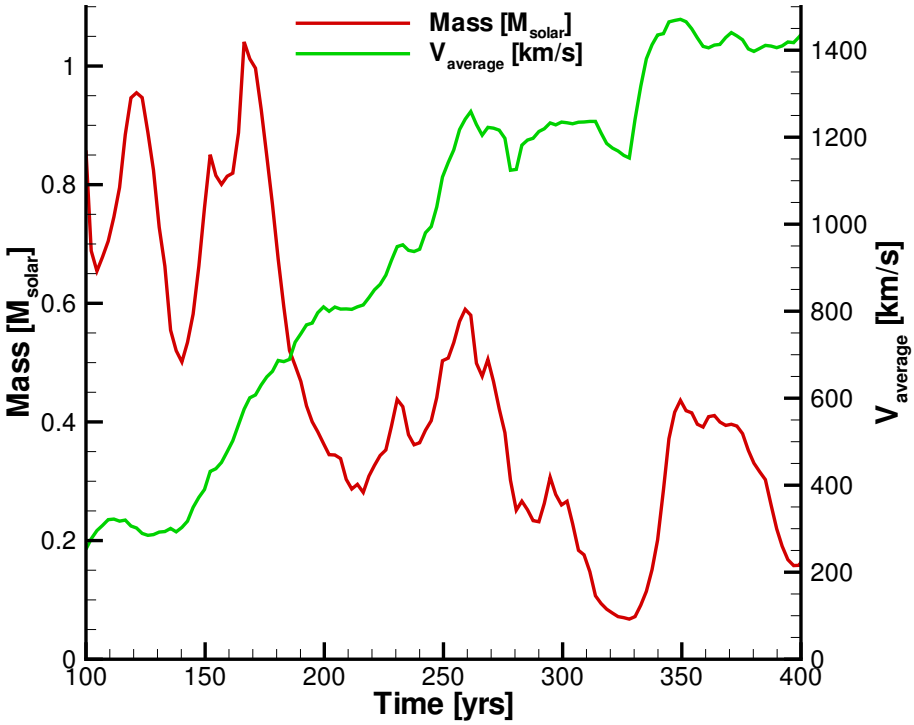

Figure 4.7: Evolution of mass in clumps and the average velocity of the clumps.

Figure 4.9 shows the position and velocities of the forward (solid) and reverse shock (dashed). In the figure showing the velocities it can be seen that both the forward and reverse shock are decelerating. The expansion parameter δ is equal to 0.66 in the figure. During the ED phase the expansion parameter is equal to 1 and at the end of the ST phase it is 0.4, so this means that our resulting SNR is currently in the ST phase. In Model 1 the SNR was already at the end of the ST phase. This difference in expansion parameter comes from the difference in time at which the supernova ejecta collided with the WR shell. In Model 1 the WR shell contained more mass, which made it more difficult to accelerate the shell. This caused the kinetic energy of the supernova ejecta to be converted into thermal energy faster and caused the expansion of the SNR to enter the pressure dominated phase earlier.

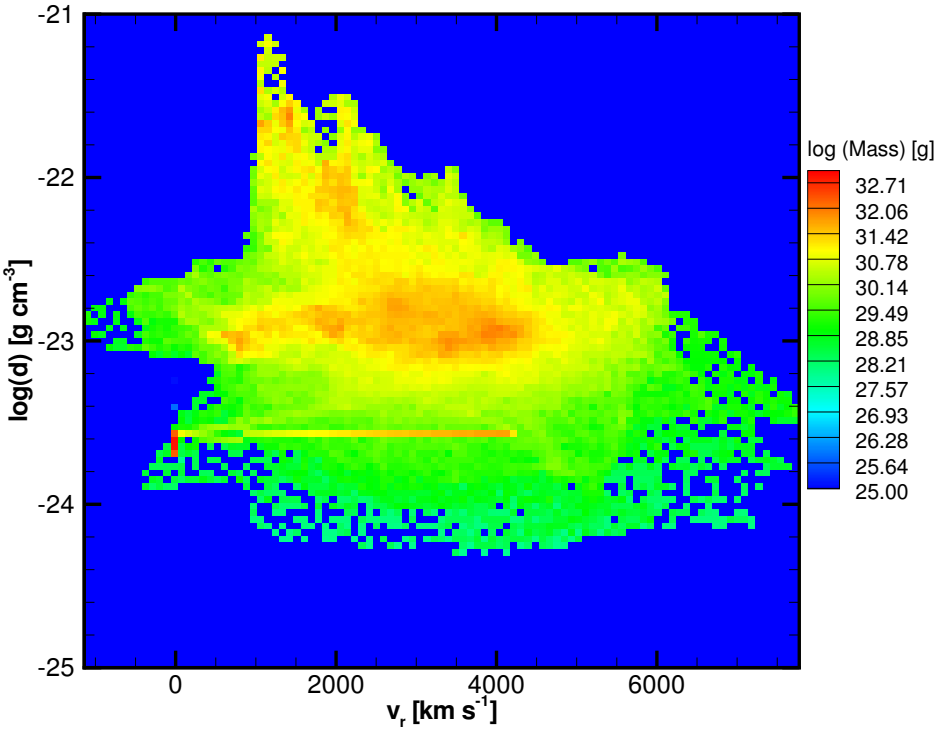

Figure 4.8: Mass distribution showing the amount of mass in a pixel corresponding to a certain range in velocity and density. The colors represent an amount of mass in each pixel, and the corresponding values can be seen in the color bar next to the figure.

4.4 Comparison with Observations

As mentioned at the end of Section 4.3.2, the comparison of the results of Model 1 with the observations of Cas A shows some important differences regarding the position and velocity of both the forward and reverse shock. The results of Model 2 reproduce the observed values for Cas A better. The velocity of the forward shock 325 years after the explosion from the Model 2 is equal to 5100 km/s. This corresponds well to the measured value of 5000 km/s (Koralesky et al. 1998). The reverse shock velocity is measured as 3000 km/s (Morse et al. 2004) which does not correspond to Model 1, 1100 km/s, or Model 2, -600 km/s.

The remains of the clumps of the WR shell are thought to be QSF in the Cas A SNR. In Model 1 the velocity spread of these clumps coincides with the observations, which give values below 500 km/s. In Model 2 the

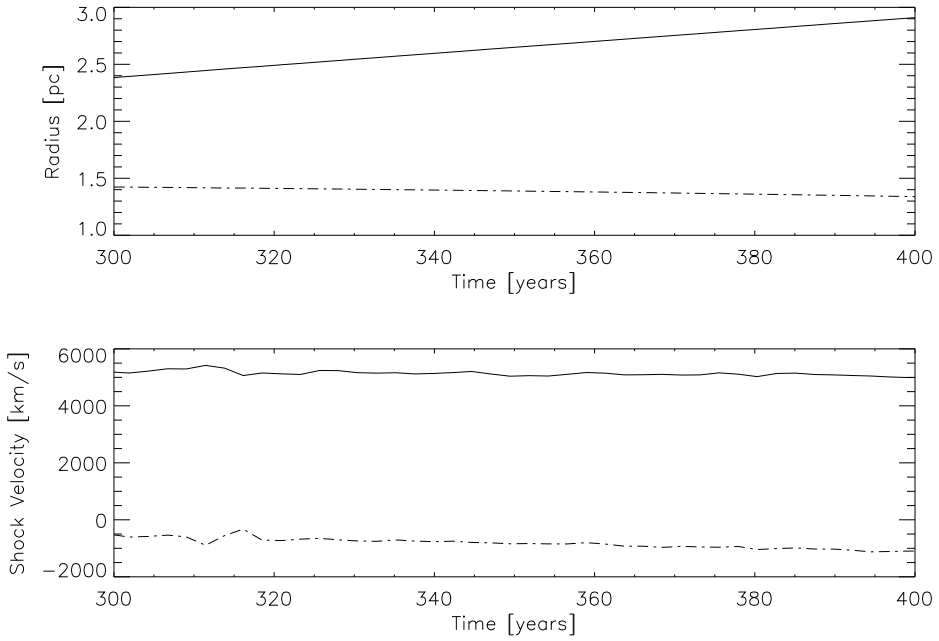

Figure 4.9: Position of the forward (solid) and reverse shock (dashed) and corresponding velocities for model 2

velocities of the clumps range from approximately 900 to 1800 km/s, which is much higher than the observed values. This difference in velocity of the clumps in the two models comes from the difference in time at which the supernova ejecta collided with the WR shell. Regarding the velocity of the high density clumps, the results of Model 1 corresponds better with the observations, assuming the clumps can be linked to the QSF in the Cas A SNR.

The high density clumps do not necessarily have to be linked to the QSF in Cas A. DeLaney et al. (2004) analyzed 261 knots observed in the X-ray regime and classified them into 4 spectral classes, Silicon dominated knots, Iron dominated knots, low energy enhanced knots and continuum dominated knots. They find that the third spectral class, which radiates more at lower energies compared to the other spectral classes, moves with a distinctly lower expansion rate.

To compare this with our model we looked at the mass distribution in the plane of radial expansion rate versus temperature and the plane of radial expansion rate versus radiative energy loss. Expansion rate is a parameter more often used when looking at observational data. The expansion rate is defined as the observed velocity in the plane of the sky, divided by the radial distance from the assumed center also in the plane of the sky. Neither of

them is always equals the real radial velocity or real distance, but is modified by line of sight effects. By dividing these two values, one gets rid of these line of sight effects.

$$\text{expansion rate} = \frac{v_{r-observed}}{r_{observed}} = \frac{v_r \cdot sin\theta}{r \cdot sin\theta} = \frac{v_r}{r} \ , \tag{4.3}$$

where θ is the angle between our line of sight and a vector perpendicular to the plane of observation. If two pieces of matter now have the same expansion rate it means they are moving in a Hubble flow, which means that $v_r \propto r$, with respect to the assumed center.

In case of our two dimensional data, we do not have any line of sight effects and therefore the conversion would not be useful if we did not want to compare it with other data. The expansion rate is expressed in % yr^{-1}.

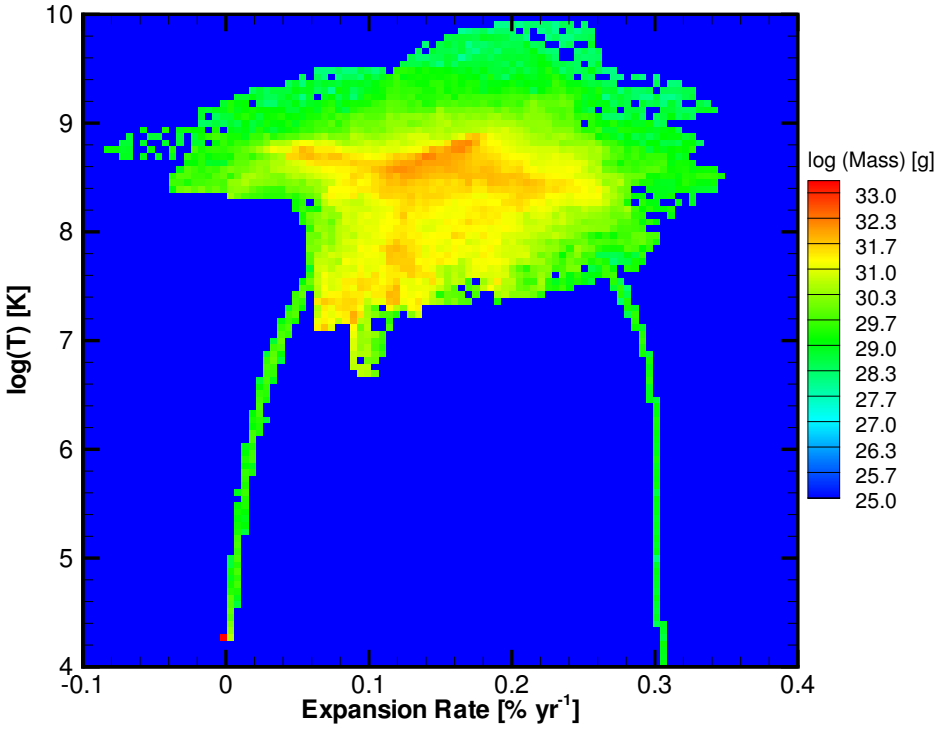

Figure 4.10: Mass distribution showing the amount of mass in a pixel corresponding to a certain range in expansion rate and temperature. The colors represent an amount of mass in each pixel, and the corresponding values can be seen in the color bar next to the figure.

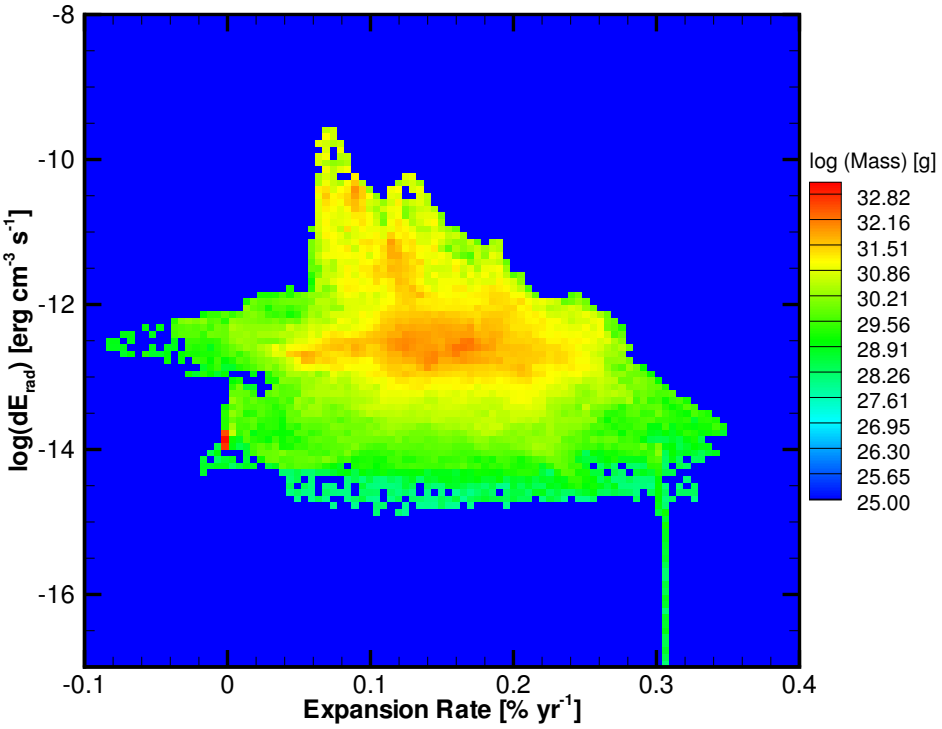

Figure 4.11: Mass distribution showing the amount of mass in a pixel corresponding to a certain range in expansion rate and radiative energy loss. The colors represent an amount of mass in each pixel, and the corresponding values can be seen in the color bar next to the figure.

Figures 4.10 and 4.11 are the mass distributions which show the amount in the plane of expansion rate versus the radiative energy loss and temperature. The two figures both show a large region with a high value for the mass within the pixel centered around an expansion rate of 0.14 % yr^{-1} and log(T) $\approx$ 8.5 or log($\mathrm{dE_{rad}}$) $\approx$ -12.5. There is also a part separated from this region which extends to lower expansion rates, lower temperatures and higher radiative energy losses, respectively.

In the mass distribution for the temperature there are two almost vertical lines, one at an expansion rate of 0 and one at 0.3. These lines are the signature of the smeared out forward and reverse shock. The same signature can be seen in the mass distribution of the expansion rate versus the radiative energy loss. In this case only the reverse shock can be seen because the matter shocked by the forward shock is radiating in the region where another

part of the grid is also radiating. The part of the grid which is in front of the forward shock can be seen as the peak in mass at zero expansion rate.

Figure 4.13 shows the mass distribution of the radiative energy loss versus the temperature. The figure shows that there is a distribution of matter which radiates at different temperatures. The high density clumps correspond to the highest radiative energy losses. The highest temperatures correspond to the lowest densities, which can be seen when comparing Figure 4.6 and Figure 4.12. The continuous distribution, which seems to originate from this peak and goes down to lower temperatures and higher energy losses, is an effect of radiative cooling. Since the cooling curve does not change much any more above 10^7 K, any parcel of matter which cools a bit and increases in density will increase the amount of radiative cooling. The peak in the mass distribution at $\log(T) \approx 4.5$ is the part of the grid outside the forward shock.

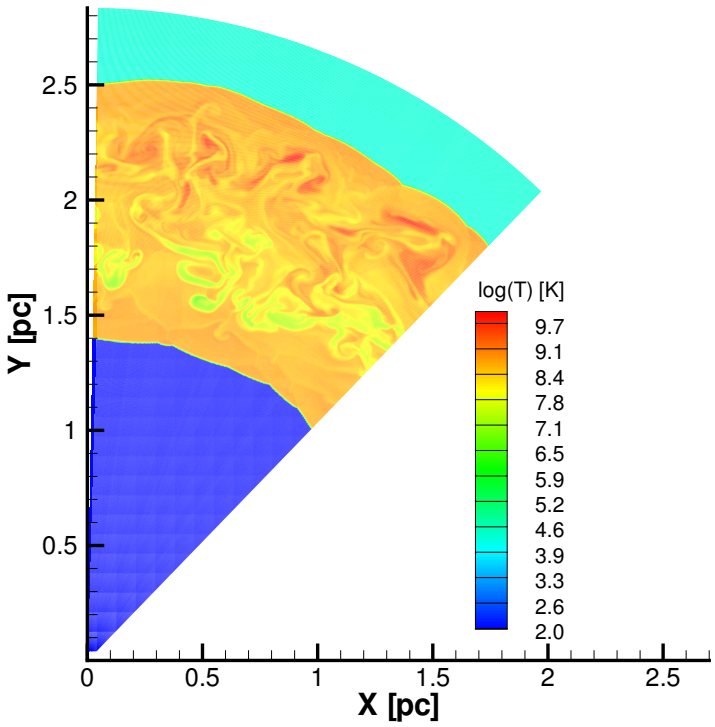

Figure 4.12: Resulting temperature structure of the CSM of model 2, 325 years after the supernova explosion. Which values of the temperature correspond to which color is shown in the colorbar in the figure.

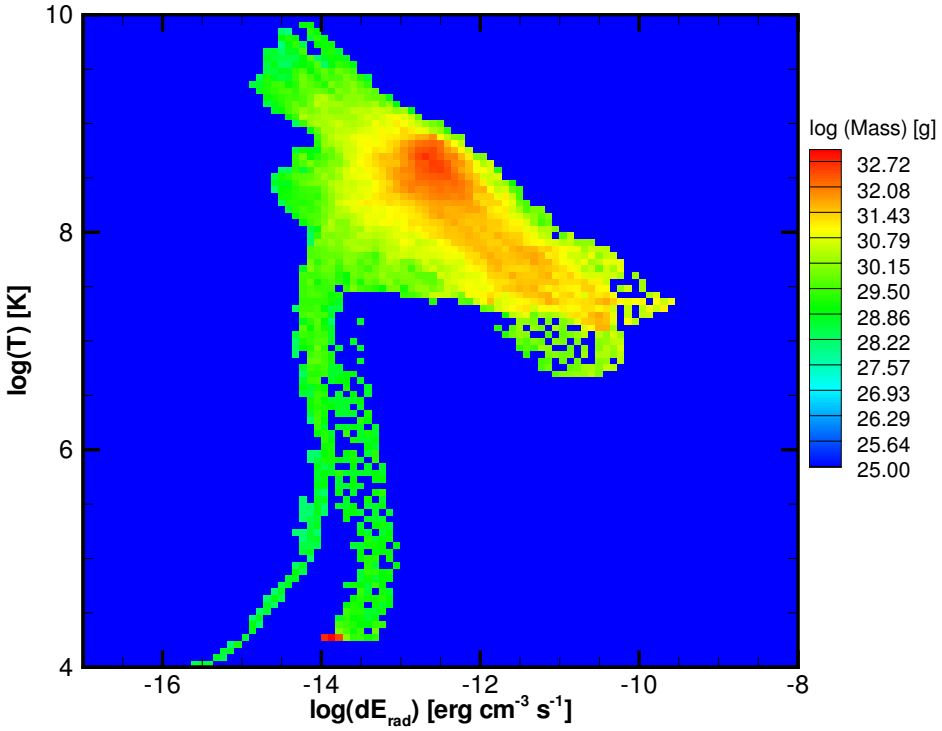

Figure 4.13: Mass distribution showing the amount of mass in a pixel corresponding to a certain range in radiative energy loss and temperature. Which value for the amount of mass in a pixel corresponds to which color is shown in the colorbar in the figure.

By looking at the Figures 4.8, 4.10 and 4.11 one could conclude that there is a component which moves slower and radiates at lower temperatures, with respect to the majority of the SNR. If one assumes that all the radiation lost is thermal radiation, it means that there is a component which moves slower and radiates more at lower energies. This would be a similar result as seen in Figure 3 of DeLaney et al. (2004).

However, one can not say that the distinct features in each mass distribution connect to the one single feature in our result for the model of Cas A. This can only be checked with help of the CSM structure in terms of the density, radiative energy loss and temperature, which are shown in Figure 4.6, 4.12 and 4.15.

By looking at Figure 4.6 and 4.8, we can see that the part of the mass distribution with the highest density, above 10^{-22} g cm^{-3}, corresponds to

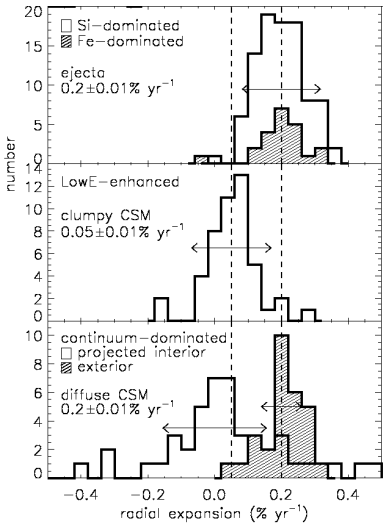

Figure 4.14: Figure taken from DeLaney et al. (2004). The x-axis is in radial expansion which is the same as the expansion rate in our results. The y-axis is in arbitrary units and cannot be quantitatively compared with the results of our model.

the high density clumps. This part moves with a lower velocity than the majority of the mass in the SNR. Comparing Figure 4.15 and 4.11, tells us that the part of the mass distribution with a radiative energy loss higher than $10^{-10.5}$ erg cm^{-3} s^{-1}, can be linked to the high density clumps. This part again moves at a lower velocity than the majority of the mass in the SNR. And finally, looking at Figure 4.12 and 4.10, we learn that the part of the mass distribution, with a temperature lower than 10^8 K, which can not be linked to the shocks, *can* be linked to the high density clumps. And also this mass in the mass distribution moves at a lower velocity than the majority of the mass in the SNR. One can thus conclude that the high density clumps move with a lower velocity, and, since they have a lower temperature, radiate more at lower energies with respect to the majority of the SNR. The expansion rate of these clumps ranges from 0.06 to 0.1 % yr^{-1}. Although this does not correspond perfectly to the range of allowed values from DeLaney et al. (2004), -0.1...0.1 % yr^{-1}, the difference is not large and may be attributed to the fact that the simulations are done only in the r, φ plane.

4.5 Conclusions

Our goal was to test the single star model as a progenitor model for the Cas A SNR. We chose a set of parameters describing the wind of the progenitor

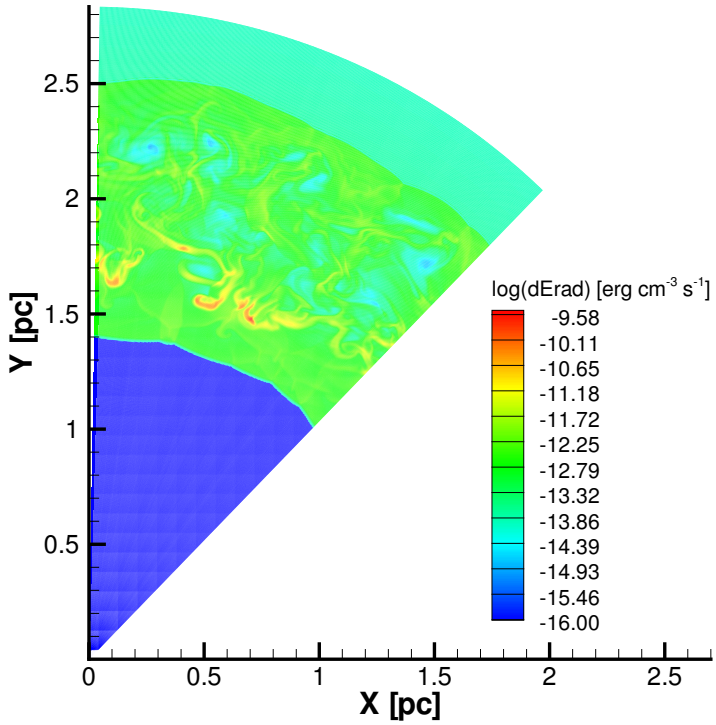

Figure 4.15: Resulting radiative energy loss profile of the SNR of model 2, 325 years after the supernova explosion

and simulated the evolution of the CSM using these parameters. The result of the pre-supernova evolution of the CSM showed a clumpy WR shell at a distance from the center. These clumps were thought to be the origin of the QSF in Cas A. After the simulation of the pre-supernova evolution of the CSM we simulated the interaction of the supernova ejecta with the CSM and obtained results for 2 models, with different WR life times. Model 1 had a WR life time of 17700 years, and Model 2 had a WR life time of 11400 years. Since the large scale structure of the SNR, position and velocity of forward and reverse shock, was not consistent with the observations for Model 1, we focus here on the results of Model 2.

The position of the forward shock, reverse shock and velocity of the forward shock in Model 2 are all consistent with the observations. Only the velocity of the reverse shock in our results was not well reproduced. The observations show a velocity of 3000 km/s, while our result gave -600 km/s. To be able to obtain the observed velocity of the reverse shock the collision

of the supernova ejecta with the WR shell would have to take place at a later time. However, the position and velocity of the forward shock would not be consistent with the observations any more if we were to change the timing of the collision. This can be seen in the result of Model 1. In Model 1 the collision did take place at a later time, and it can be seen that the velocity of the reverse shock corresponds better to the observed value for Model 1 than it does for Model 2.

Originally we wanted to link the high density clumps in the result with the QSF from Cas A. In Model 2 the velocity of these clumps was inconsistent with the observed velocities for the QSF. In Model 1, there were velocities which were consistent with the observations but there were also velocities which were too high. The collision of the supernova ejecta with the WR shell causes the clumps in the WR shell to be accelerated and partly stripped of mass. If the collision of the supernova ejecta with the WR shell took place at an earlier time, the effect of the acceleration and mass stripping will be larger. The fact that we obtain too high velocities could thus be a result of the collision taking place too early.

If the radial distribution of the clumps in the WR shell would have been larger, the interaction of the supernova ejecta with these clumps would take place at different times, and the distribution of velocities would also extend to smaller velocities. This could solve the problem of the high velocities. Only the clumps which had an interaction with the supernova ejecta recently would be observed as QSF.

The observed asymmetry in the supernova ejecta could also be used to explain the high velocities. At a certain place the interaction of the supernova ejecta with the clumps has already taken place but at another this has only just happened. The results of Model 2 would then correspond to a position where the interaction has already taken place long ago. The places where the interaction would only just have happened would show clumps with lower velocities.

The high density clumps in the results of Model 2 can also be linked to another observational feature in the Cas A SNR. The figures with the mass distributions showed that the clumps move at a lower velocity, have a lower temperature and a higher radiative energy loss compared to the rest of the remnant. This has also been seen by DeLaney et al. (2004), who find a subclass in the X-ray emitting part of Cas A which moves slower and radiates more at lower energies. We think that the high density clumps in the results of Model 2 might correspond to this observational feature in stead of the QSF. However, this would mean that the origin of the QSF remains unknown.

In Model 2 we were able to reproduce the large scale structure, the shock positions and velocities, and find a correlation between the smaller scale structure of our result and some of the observations done, the high density clumps. Although there are still unresolved issues, we think the single star

model has passed the test and can be considered as a serious candidate for the progenitor of Cas A.

Since the ZEUS3D code does not track elemental abundances, it is hard to distinguish what was part of the CSM and what was part of the supernova ejecta. It would be very useful to have this information since that would make the comparison between the results and the observations much easier.

Chapter 5

Review

5.1 Looking back

With help of the ZEUS3D code and an assumed profile for the supernova ejecta, we developed a method to simulate the interaction of supernova ejecta with an evolved CSM. In Chapter 2 we described this method. In Chapter 3 we took a model for the progenitor evolution of SN 2001em, and saw that the method gave results similar to other methods. Besides this, the results we obtained also reproduced some of the observations. In Chapter 4 we simulated the evolution of the CSM of the progenitor star of Cas A with a model which we thoroughly discussed. The resulting interaction of the supernova ejecta with the evolved CSM showed that the single star progenitor model for Cas A is a serious candidate. The results also showed a strong correspondence of an observational feature in Cas A, a component which moves slower and radiates more at lower energies, which could be linked to the clumps originating from the instabilities in the WR shell.

5.2 Looking Forward

Various physical processes have not been included in this thesis. One, which could be important in supernovae, is cosmic ray acceleration across shocks. In general non-thermal radiation processes are also not included. How the addition of these processes would affect the evolution of supernovae in general is hard to say. The effects would have to be considered for each case separately.

To be able to obtain results that can be compared better with observations, the first improvement that will be useful is the addition of elemental abundances. With this addition we are able to determine what is part of the supernova ejecta and what was a part of the CSM, long after the violent interaction of both. This will of course only be useful if we compare with supernovae which we can spatially resolve.

An improvement in the radiative energy loss in general would improve the results. Radiative transfer would give ionization states of different elements and the inclusion of the elemental abundance would give the composition. With these two additions the cooling function could be improved in such a way that it would be possible to get more detailed light curves and perhaps even spectra. This would be particularly useful for comparison with supernovae which we do no spatially resolve.

In this thesis the parameter n, which indicated the slope of the declining density profile, has been kept constant. As mentioned in Chapter 2, this value is dependent on the density profile of the progenitor star. It would be useful to see how the results we obtained would depend on this parameter.

Ultimately it would be nice to obtain detailed results of supernova explosion, starting from the core collapse, and put these in the evolved CSM of the progenitor star. Since the mechanism which causes the ejection of the matter is not yet completely understood, this endeavor is still too ambitious.

If the above mentioned addition would be made to the code, it could be to, by looking at the SNR, constrain the evolution of the progenitor star. This would have implications on stellar evolution models. Which star can or can not end up as a supernova? Which phases has the star gone through during its life? Questions like these might be answered.

Acknowledgements

I would like to thank several people. First and foremost I want to thank Norbert Langer. His guidance throughout the year in which I did my Masters research helped me to get to the point where I am now. His always present, but justified and usefull critisism, helped me to see my errors and understand them. Lots of thanks go out to Jacco Vink, whose contribution in the discussion regarding Cas A provided more insights. Also thanks go out to Allard-Jan van Marle, whom I frequently bother with all kinds of question, and was always willing to help. Finally I would also like to thank Guillermo Garcia-Segura and Carlos Badenes for taking time to aid me through email and when they were visiting the Netherlands.

Bibliography

Allen, A. J. & Hughes, P. A. 1984, MNRAS, 208, 609

Chevalier, R. A. 1977, ARA&A, 15, 175

Chevalier, R. A. 1982, ApJ, 259, L85

Chevalier, R. A. & Oishi, J. 2003, ApJ, 593, L23

Chugai, N. N. & Chevalier, R. A. 2006, ApJ, 641, 1051

da Silva, L. A. L. 1993, Astrophys. Space Sci., 202, 215

de Jager, C., Nieuwenhuijzen, H., & van der Hucht, K. A. 1988, A&A Suppl., 72, 259

DeLaney, T., Rudnick, L., Fesen, R. A., et al. 2004, ApJ, 613, 343

Dwarkadas, V. V. 2005, ApJ, 630, 892

Fesen, R. A., Morse, J. A., Chevalier, R. A., et al. 2001, AJ, 122, 2644

Garcia-Segura, G., Langer, N., & Mac Low, M.-M. 1996, A&A, 316, 133

García-Segura, G., Langer, N., Różyczka, M., & Franco, J. 1999, ApJ, 517, 767

Ghavamian, P., Hughes, J. P., & Williams, T. B. 2005, ApJ, 635, 365

Gotthelf, E. V., Koralesky, B., Rudnick, L., et al. 2001, ApJ, 552, L39

Granot, J. & Ramirez-Ruiz, E. 2004, ApJ, 609, L9

Hirschi, R., Meynet, G., & Maeder, A. 2004, A&A, 425, 649

Iben, I. J. & Livio, M. 1993, PASP, 105, 1373

Kifonidis, K., Plewa, T., Janka, H.-T., & Müller, E. 2003, A&A, 408, 621

Kippenhahn, R. & Weigert, A. 1990, Stellar Structure and Evolution (Stellar Structure and Evolution, XVI, 468 pp. 192 figs.. Springer-Verlag Berlin Heidelberg New York. Also Astronomy and Astrophysics Library)

Koralesky, B., Rudnick, L., Gotthelf, E. V., & Keohane, J. W. 1998, ApJ, 505, L27+

Kwok, S. 2000, The Origin and Evolution of Planetary Nebulae (The origin and evolution of planetary nebulae / Sun Kwok. Cambridge ; New York : Cambridge University Press, 2000. (Cambridge astrophysics series ; 33))

MacDonald, J. & Bailey, M. E. 1981, MNRAS, 197, 995

Matzner, C. D. & McKee, C. F. 1999, ApJ, 510, 379

McKee, C. F. 1974, ApJ, 188, 335

Mereghetti, S., Tiengo, A., & Israel, G. L. 2002, ApJ, 569, 275

Meyer, F. 1997, MNRAS, 285, L11

Meynet, G. & Maeder, A. 2005, A&A, 429, 581

Morse, J. A., Fesen, R. A., Chevalier, R. A., et al. 2004, ApJ, 614, 727

Nomoto, K., Thielemann, F.-K., & Yokoi, K. 1984, ApJ, 286, 644

Nugis, T. & Lamers, H. J. G. L. M. 2000, A&A, 360, 227

Papenkova, M., Li, W. D., Wray, J., Chleborad, C. W., & Schwartz, M. 2001, IAU Circ., 7722, 1

Pooley, D. & Lewin, W. H. G. 2004, IAU Circ., 8323, 2

Reed, J. E., Hester, J. J., Fabian, A. C., & Winkler, P. F. 1995, ApJ, 440, 706

Ryu, D. & Vishniac, E. T. 1988, ApJ, 331, 350

Salasnich, B., Bressan, A., & Chiosi, C. 1999, A&A, 342, 131

Soderberg, A. M., Gal-Yam, A., & Kulkarni, S. R. 2004, GRB Coordinates Network, 2586, 1

Stockdale, C. J., Kaster, B., Sjouwerman, L. O., et al. 2005, IAU Circ., 8472, 4

Stockdale, C. J., Van Dyk, S. D., Sramek, R. A., et al. 2004, IAU Circ., 8282, 2

Stone, J. M. & Norman, M. L. 1992, ApJS, 80, 753

Tananbaum, H. 1999, IAU Circ., 7246, 1

Thorstensen, J. R., Fesen, R. A., & van den Bergh, S. 2001, AJ, 122, 297

Truelove, J. K. & McKee, C. F. 1999, ApJS, 120, 299

van den Bergh, S. 1971, ApJ, 165, 457

Vink, J. 2004, New Astronomy Review, 48, 61

Vink, J., Kaastra, J. S., & Bleeker, J. A. M. 1996, A&A, 307, L41

Weaver, R., McCray, R., Castor, J., Shapiro, P., & Moore, R. 1977, ApJ, 218, 377

Willingale, R., Bleeker, J. A. M., van der Heyden, K. J., & Kaastra, J. S. 2003, A&A, 398, 1021

Winkler, P. F. & Kirshner, R. P. 1985, ApJ, 299, 981

Woltjer, L. 1972, ARA&A, 10, 129

Woosley, S. E., Langer, N., & Weaver, T. A. 1993, ApJ, 411, 823

Yorke, H. W., Bodenheimer, P., & Taam, R. E. 1995, ApJ, 451, 308

Young, P. A., Fryer, C. L., Hungerford, A., et al. 2006, ApJ, 640, 891